Title: Widespread ripples synchronize human cortical activity

Authors: Charles W. Dickey[1,2,*], Ilya A. Verzhbinsky[2], Xi Jiang[1], Burke Q. Rosen[1], Sophie Kajfez[3], Brittany Stedelin[4], Jerry J. Shih[5], Sharona Ben-Haim[6], Ahmed M. Raslan[4], Joseph R. Madsen[7], Emad N. Eskandar[8], Jorge Gonzalez-Martinez[9], Sydney S. Cash[10], Eric Halgren[3,5,*]

Affiliations:
[1]Neurosciences Graduate Program, University of California San Diego, La Jolla, CA 92093, USA
[2]Medical Scientist Training Program, University of California San Diego, La Jolla, CA 92093, USA
[3]Department of Radiology, University of California San Diego, La Jolla, CA 92093, USA
[4]Department of Neurological Surgery, Oregon Health & Science University, Portland, OR 97239, USA
[5]Department of Neurosciences, University of California San Diego, La Jolla, CA 92093, USA
[6]Department of Neurological Surgery, University of California San Diego, La Jolla, CA 92093, USA
[7]Division of Epilepsy Surgery, Department of Neurosurgery, Boston Children's Hospital, Harvard Medical School, Boston, MA 02115, USA
[8]Department of Neurological Surgery, Montefiore Medical Center, Albert Einstein College of Medicine, Bronx, NY 10461, USA
[9]Epilepsy Center, Cleveland Clinic, Cleveland, OH 44106
[10]Department of Neurology, Massachusetts General Hospital, Harvard Medical School, Boston, MA 02114, USA
*Corresponding authors: Eric Halgren (ehalgren@health.ucsd.edu), Charles W. Dickey (cdickey@health.ucsd.edu)

Acknowledgements: We thank Adam Niese, Christine Smith, Christopher Gonzalez, Daniel Cleary, Eran Mukamel, Erik Kaestner, Jacob Garrett, Maxim Bazhenov, Terrence Sejnowski, and Zarek Siegel for their support. This work was supported by NIMH (1RF1MH117155-01, T32 MH020002) and ONR-MURI (N00014-16-1-2829).

Author contributions: C.D. and E.H. designed the study. C.D., B.S., J.S., S.B., A.R., J.M., E.E., J.G., and S.C. collected the data. C.D., I.V., and X.J. analyzed the data. B.R. and S.K. provided support for the analyses. C.D. and E.H. wrote the manuscript. E.H. supervised the work.

Competing interests: The authors declare no competing interests.

Abstract

Hippocampal ripples index the reconstruction of spatiotemporal neuronal firing patterns essential for the consolidation of memories in the cortex during sleep. Here, using human intracranial recordings, we show that ~70ms long ~80Hz ripples are ubiquitous in the cortex during both waking and non-rapid eye movement sleep. During sleep, cortical ripples are generated on the down-to-upstate transition with phase-locked firing patterns suggesting generation by pyramidal-interneuron-feedback. They mark recurrence of spatiotemporal patterns from preceding waking, and group co-firing which facilitates plasticity. During waking, cortical ripples co-occur with hippocampal ripples during local activity peaks, especially preceding correct delayed memory recall. Critically, during sleep and waking, cortical ripples co-occur and phase-synchronize across widespread locations, including between hemispheres. High-gamma amplitude correlation increases between co-rippling sites, possibly indicating facilitated information exchange. Co-occurrence, phase-synchrony, and high-gamma correlation do not decrement with distance. The hippocampo-cortico-cortical co-rippling network is a novel possible substrate for event-integration in memory and cognition.

Introduction

Ripples have been extensively studied in rodent hippocampus during non-rapid eye movement (NREM) sleep, when they mark the replay of events from the prior waking period, and are critical for memory consolidation in the cortex[1-4]. They are associated with cortical replay[5-7], and with cortical sleep waves (spindles, downstates, upstates)[8], a relationship crucial for consolidation[9]. Rat hippocampal ripples comprise a ~140Hz oscillation at the peak of a ~70ms duration sharpwave, followed by a slower local potential[2]. Human sharpwave-ripples also occur during NREM with similar temporal relationships to spindles and down-upstates and hippocampal topography, but with a median frequency of 80-90Hz[10-13].

Recently, ripples were found in rat association cortex but not primary sensory or motor cortices during sleep, with increased coupling to hippocampal ripples in sleep following learning[14]. An earlier study reported ripples in waking and sleeping cat cortex, especially NREM[15]. In humans, cortical ripples during waking were more frequently found in lateral temporal than rolandic cortex, and coupled to parahippocampal gyrus ripples more often prior to correct paired-associates recall[16]. Lateral temporal units fired in-phase with the local ripples in patterns previously observed during learning[17]. Waking hippocampal ripples were also associated with cortical activity patterns selective for faces and buildings during free recall[18].

Thus, there is an emerging appreciation that, in both humans and rodents, hippocampal and cortical ripples play an important role in memory during both sleep and waking. However, many basic questions remain unresolved. Cortical ripples have not been described in human sleep, nor have their relationships to sleep spindles, downstates, and upstates been determined. Such relationships could support a role of cortical ripples in consolidation, as would associated increased co-firing within the window of spike-timing-dependent plasticity (STDP), and association with recurrence of spatiotemporal activity patterns from waking. The basic and network characteristics of ripples have not been compared between cortex and hippocampus, or between sleep and waking, so it is unclear how these may change between their putative roles of supporting consolidation vs. recall, or indeed if they represent the same phenomenon. The relationships of human cortical pyramidal and inhibitory cell-firing to ripples and to each other, important for understanding ripple generation, have not been determined. Knowledge of the distribution of ripples across different cortical areas during waking is limited and during sleep is

absent. Most importantly, nothing is known of the network properties of cortical ripples. Specifically, it is not known if they co-occur, and even phase-lock, between cortical sites, and if so, at what distance. These would be crucial properties for cortical ripples to participate in the integration of different elements of memories that are represented in distinct cortical areas.

In the current study, using human intracranial stereoelectroencephalography (SEEG) recordings, we characterize ripples throughout the cortex during waking and NREM sleep, and relate them to simultaneously-recorded hippocampal ripples. Using single-unit recordings, we identify their probable generating circuits. We show how cortical ripples in NREM are linked to spindles and down-upstates, and to the recurrence of spatiotemporal patterns from preceding waking. We found that, crucial to the hypothesized role of ripples in coordinating consolidation and retrieval of memories composed of widely-distributed elements, ripples co-occur and phase-lock across all lobes and both hemispheres without decrement with distance, and co-occur in multiple cortical and hippocampal sites preceding successful delayed recall. These characteristics suggest that distributed, phase-locked cortical ripples may assist in the integration of different components of a memory, and their coordination with sleep waves and hippocampal ripples could be central to memory recall and consolidation. More generally, such ripples may also help 'bind' different aspects of a mental event encoded in widespread cortical areas into a coherent representation.

Results

Ripples are generated across states and structures

Ripples were detected using intracranial cortical and hippocampal recordings in 17 patients undergoing monitoring for seizure focus localization (STable 1). Bipolar derivations ensured measurement of local field potentials (LFP). Ripples were detected exclusively from non-lesional, non-epileptogenic regions and were required to have at least 3 cycles of increased 70-100Hz amplitude without contamination by epileptiform activity or artifacts (SFig.1). Ripples were found during both waking and NREM sleep in all cortical areas sampled (Fig.1A-B,E-H, SFigs.2-3, STable 2), and hippocampus (Fig.1C-D, STable 3).

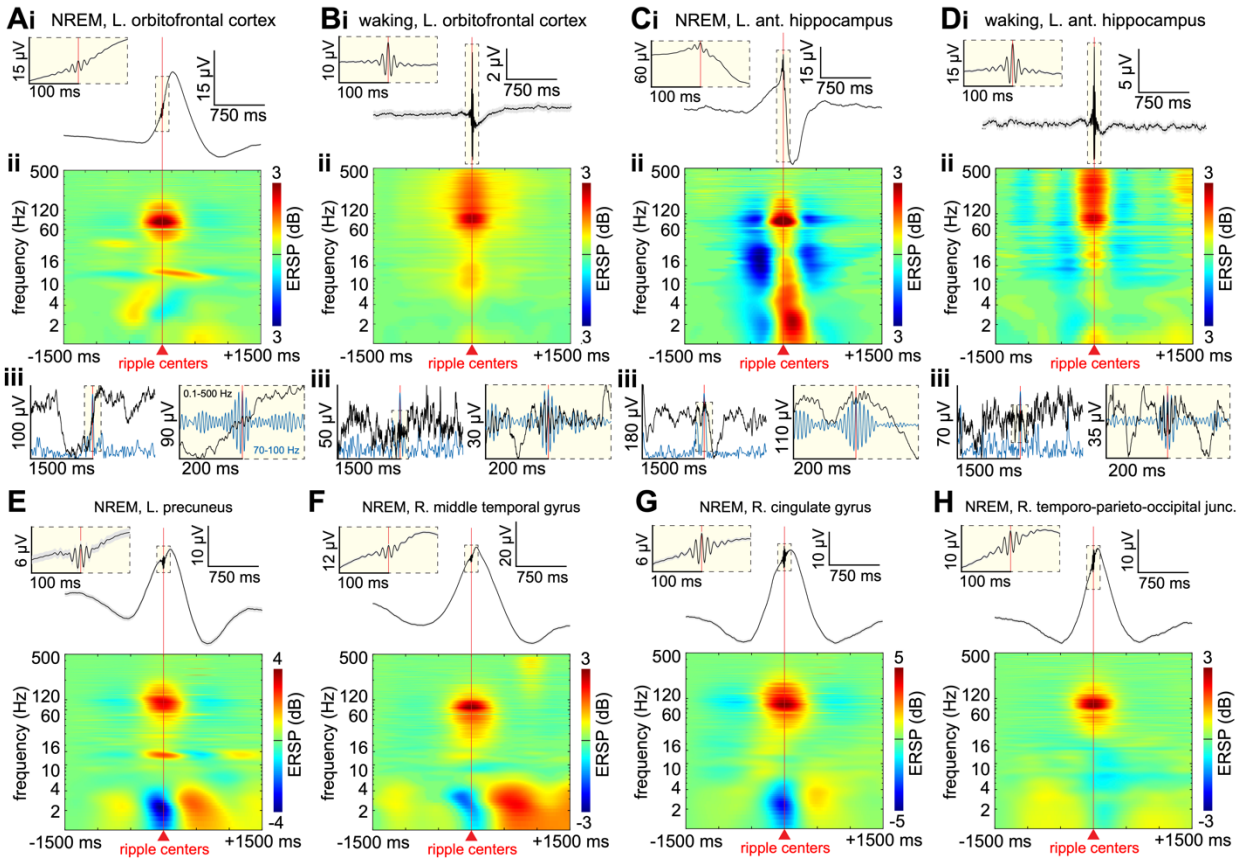

Fig. 1. Cortical and hippocampal ripples are generated during NREM sleep and waking. (**A**) Orbitofrontal average broadband LFP (**i**) and time-frequency (**ii**) across ripples, and example broadband ripple (**iii**) unfiltered sweeps (black, left–3000ms, right–400ms), and 70-100Hz bandpass (blue, left-analytic amplitude, right-sweep), from one channel during NREM sleep. (**B**) Same as (A) except during waking. (**C**) Same as (A) except hippocampal ripples. (**D**) Same as (C) except during waking. (**E-H**) Same as (A) except for other cortical regions. Note the highly consistent occurrence of cortical ripples on the upslope of the down-to-upstate transition during NREM sleep. All plots show ripples detected on trans-gray matter bipolar SEEG channels. LFP=local field potential, NREM=non-rapid eye movement, SEEG=stereoelectro-encephalography.

Across states and structures, ripple frequency was remarkably consistent (~80Hz), durations were similar (~70ms), and spontaneous cortical ripple occurrence rate was higher during NREM sleep than waking (Fig.2A). Recording epochs and channels with possible contamination by epileptiform activity were rigorously rejected, and these basic ripple characteristics were very similar when only cortical or hippocampal channels free of interictal spikes were analyzed (SFig.1B-C). Previous work in sleeping rats[14] and waking humans[16] found cortical ripples to be absent or infrequent in early sensory and motor as compared to association areas. In contrast, we found that ripple density, amplitude, and accompanying >200Hz amplitude (a proxy for unit-firing[19]), were all lower in association areas, as indicated by a positive correlation with the myelination index[20] (Fig.2C, SFig.4).

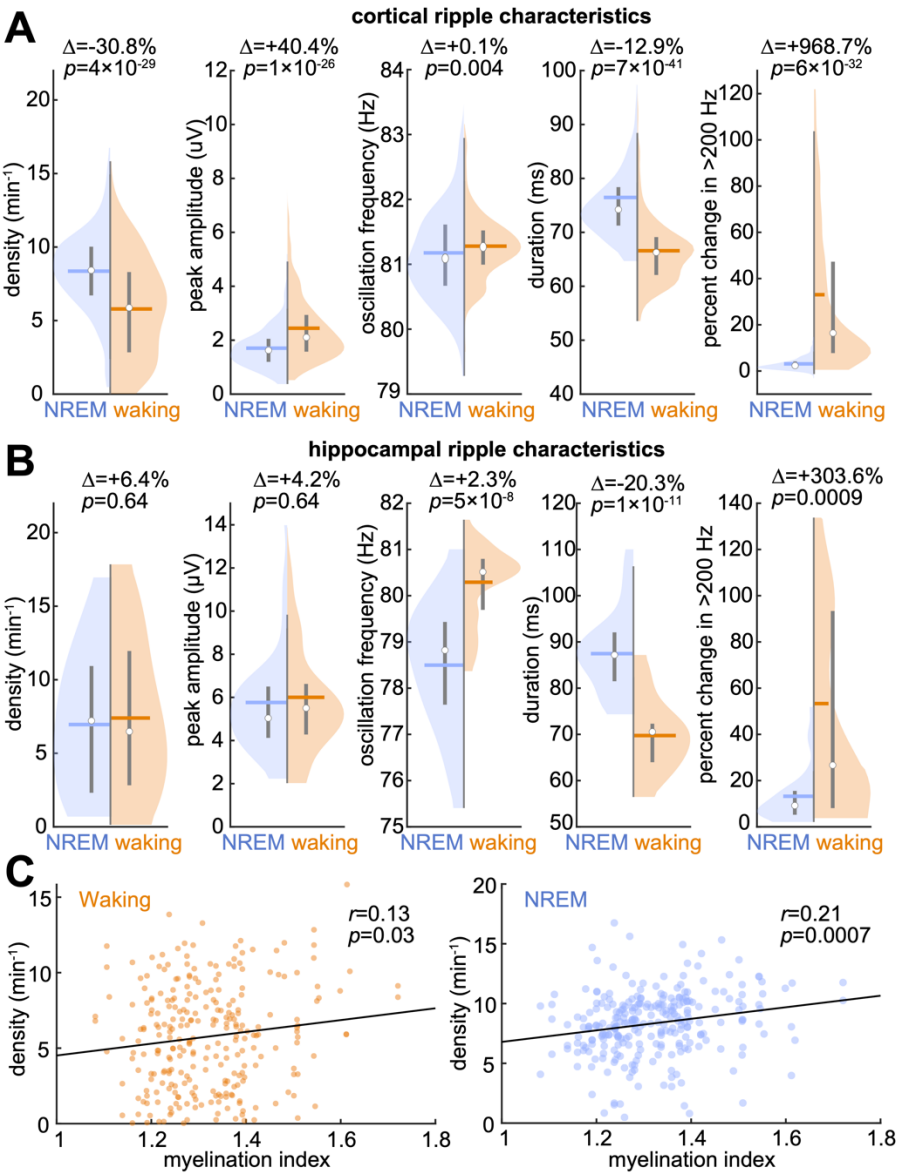

Fig. 2. Cortical and hippocampal ripple characteristics. (**A**) NREM sleep vs. waking cortical ripple density, peak 70-100Hz amplitude, frequency, duration, and percent change in mean >200Hz amplitude during ripples compared to a -2 to -1s baseline (*N*=273 channels; SEEG patients S1-17). (**B**) Same as (A) except hippocampal ripples (*N*=28 channels). Circles show medians; horizontal lines, means; vertical lines, interquartile ranges. FDR-corrected *p*-values, two-sided paired *t*-test. (**C**) Cortical ripple density was positively correlated with cortical parcel myelination index (i.e., lower in association areas[20]), as were amplitude, frequency, and accompanying >200Hz amplitude (SFig.4). FDR=false discovery rate.

Cortical ripples lock to NREM sleep waves involved in memory consolidation

NREM sleep is characterized by large downstates, often followed by upstates with spindles[21,22]. Hippocampal ripples tend to occur on the cortical down-to-upstate transition with spindles in rodents[7,8] and humans[10,11]. Cortical ripples occur on upstate and spindle peaks in cats[15] and rats[14]. In humans, we found that cortical ripples were generated during down-to-upstate

transitions (Fig.1A,E-H, Fig.3A-B,D, SFig.3A-B), often during spindles (Fig.3A,C; STables 4-5), with a preference for spindles preceding upstates (SFig.5).

Pyramidal-preceding-interneuron spiking phase-locks to cortical ripples

In humans, upstates[23] and spindles[24] induce strongly increased unit-firing. Using microelectrode array recordings from granular/supragranular layers of lateral temporal cortex during NREM sleep (SFig.3A, STable 6), we found unit firing-rates also increased during ripples (Fig.3E-F). The increased firing during ripples in NREM sleep and their occurrence on upstates and spindles implies an underlying phasic depolarization, which can generate ~80Hz oscillations in computational and experimental models via pyramidal-interneuron feedback inhibition[2,25]. Depolarization causes basket cells to fire synchronously, inhibiting other basket cells and pyramids via $GABA_A$. Pyramids fire upon recovery, exciting basket cells as they recover, leading to another cycle. As predicted, we found that pyramids and interneurons were strongly phase-locked to cortical ripples (Fig.3E), with pyramidal significantly leading interneuron spiking (Fig.3G-H). Furthermore, interneurons fired at ripple peak, when pyramidal somatic inhibition would be maximal, as found in cats[15]. Similarly, ripple amplitude was higher in waking than NREM sleep (Fig.2A), consistent with relative depolarization of pyramidal membrane potential during waking. Phasic depolarization during waking ripples was also suggested by increased >200Hz amplitude (Fig.2A-B). Thus, human cortical ripples are associated with strong tonic and phase-locked increases in pyramidal and interneuron firing rates, and are likely generated by a sudden depolarization triggering pyramidal-interneuron feedback oscillations. The increased firing, and especially its phase-concentration, produced short latency co-firing (STable 7), which provides a necessary and sufficient condition for STDP, and therefore may underlie the crucial contribution of these nested waves to consolidation[24].

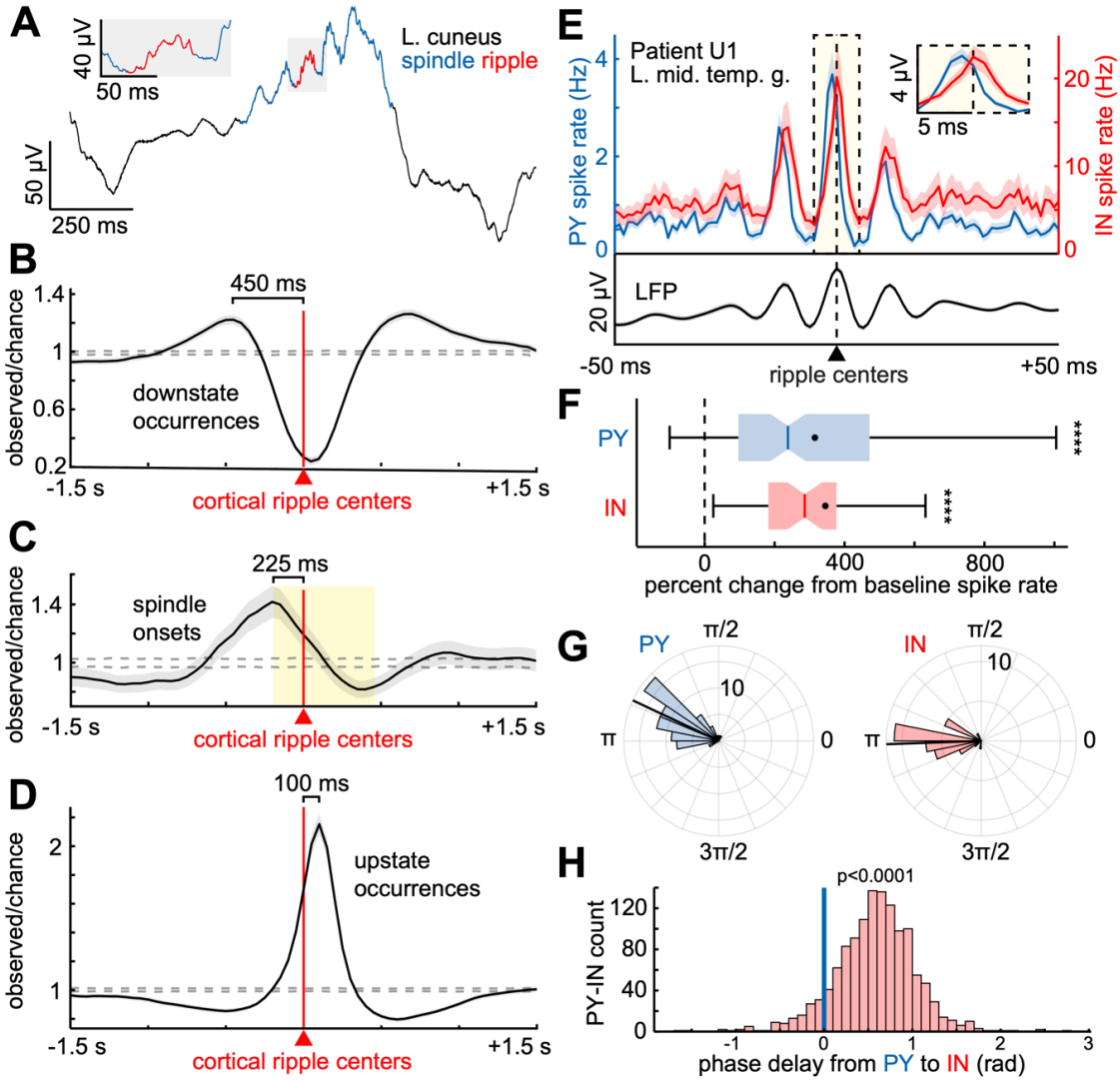

Fig. 3. Cortical ripple relationships to sleep waves and single unit spiking. (**A**) Example cortical ripple occuring during a spindle on a down-to-upstate transition. (**B**) Average downstate peak times plotted relative to local cortical ripple centers at *t*=0 across significant channels (*N*=258/273, patients S1-17). Dashed lines show 99% confidence interval of the null distribution (200 shuffles/channel). (**C-D**) Same as (B) except spindle onsets (*N*=80/273) (**C**) with shaded area indicating average spindle duration and downstate peaks (*N*=260/273) (**D**). (**E**) Mean broadband cortical ripples (black) and associated local PY (*N*=69) and IN (*N*=23) spike rates during NREM sleep. (**F**) Single unit spike rates increase during cortical ripples (PY: *N*=133, mean=315%; IN: *N*=38, mean=345%; patients U1-3). (**G**) Circular mean 70-100Hz phase of spikes of each PY (*N*=73, mean=2.70rad, $p=2\times10^{-7}$, Hodges-Ajne test) and IN (*N*=36, mean=3.18rad, p≈0) during local cortical ripples (minimum 30 spikes per unit). PY spiking preceded IN spiking by 0.48rad ($p=2\times10^{-7}$, Watson-Williams test). (**H**) Circular mean ripple phase-lags of spikes from each PY (*N*=73) to each IN (*N*=36) (*N*=1280 unit pairs, mean=0.58±0.46rad, $p=1\times10^{-268}$, one-sample one-sided *t*-test). IN=putative interneuron, PY=putative pyramidal.

Cortical ripples mark 'replay' of spatiotemporal activity patterns

Hippocampal ripples in NREM sleep mark the assembly of spatiotemporal firing patterns reproducing the sequential attributes of events from the preceding waking, supporting cortical replay and consolidation[2,26]. However, cortical ripples have not been associated with replay during NREM sleep. Our group previously identified waking spatiotemporal patterns of high gamma (70-190Hz) activity across widespread cortical areas that recurred more often in the following compared to preceding sleep night (Fig.4A). These events also coupled to upstates, spindles and hippocampal ripples[27]. In new analyses of these data (STable 8), we found that the high gamma events that comprised these sequences of putative replay were strongly linked to cortical ripples (Fig.4B-E).

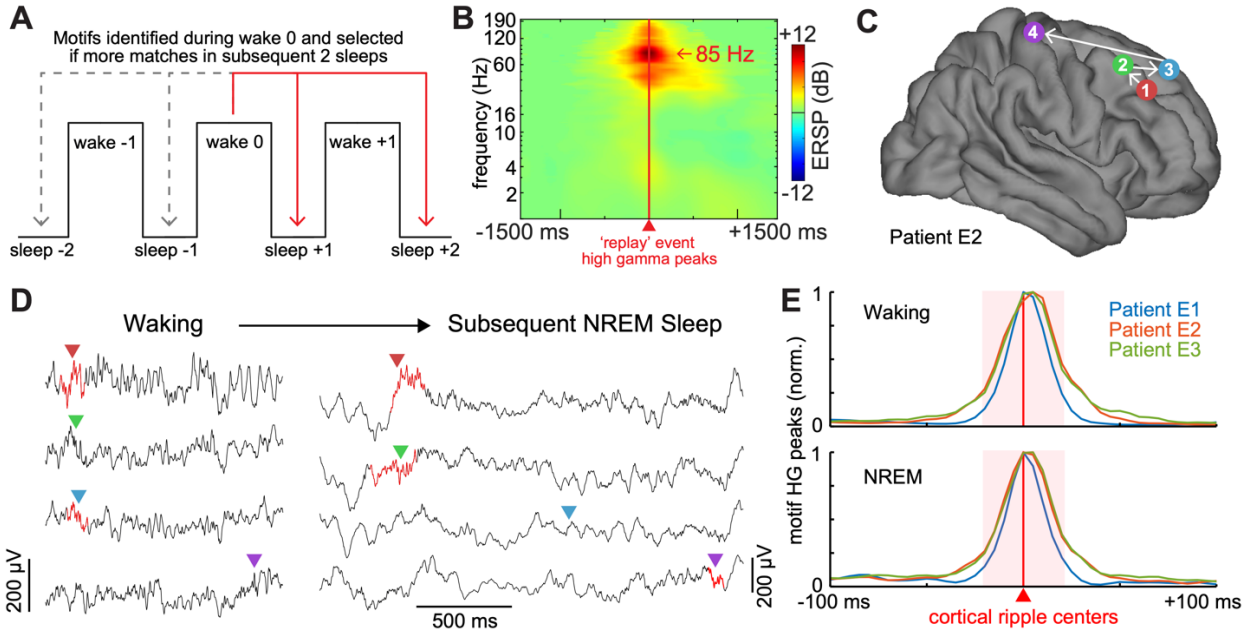

Fig. 4. Cortical ripples during NREM sleep are associated with spatiotemporal activity patterns that recur from previous waking. (**A**) Spatiotemporal patterns ('Motifs') of high gamma were identified during waking and those that occurred more during the subsequent compared to the previous 2 overnight sleeps were selected for analysis[27]. (**B**) Average time-frequency plot centered on Motif high gamma peaks shows focal activation in the ripple band. (**C-D**) Spatiotemporal high gamma peak sequence from an example Motif superimposed on a template brain (**C**) and as broadband LFP traces with ripples indicated in red (**D**). (**E**) Average Motif high gamma peak times plotted relative to local cortical ripple centers.

Cortical ripples co-occur across widespread regions

Hippocampal sharpwave-ripple occurrence and ripple coupling between parahippocampal gyrus and temporal association cortex are increased preceding memory recall in humans[16,18], possibly facilitated through the replay of cortical neuron firing sequences established during encoding[17]. In rats, cortical ripples co-occurred between hippocampus and ~1mm^2 of parietal cortex in sleep following learning[14], and in cats, ripple co-occurrence was limited to short distances[15]. Here, we demonstrate that, in addition to hippocampo-cortical coupling (Fig.5B), cortical ripples have frequent and strong coupling (occurrence within ±500ms), between all cortical areas sampled (Fig.5A, STable 9), including between hemispheres. These results remained consistent when only cortical and hippocampal channels that were free of interictal spikes were analyzed

(STable 9). Short latency coupling led to ripple co-occurrence (overlapping ≥25ms), which was greater during waking than NREM sleep (Fig.5C, STable 10). Two cortical sites co-rippling made it more likely for other sites also to co-ripple (STable 11), with multiple (>2) locations co-rippling at a much higher rate than would be expected from chance (Fig.5D, SFig.6). Critically, cortical ripple co-occurrence was not associated with distance (Fig.5E, STable 12), but rather was widely distributed across lobes and hemispheres, consistent with a role in co-activation of the diverse elements constituting a memory.

Cortical ripples co-occur with hippocampal spindle-ripples, and follow sharpwave-ripples

In humans, anterior hippocampal ripples often occur on sharpwaves[11], whereas posterior hippocampal ripples are often associated with spindles[12]. Sharpwave-ripples are more associated with sleep waves in prefrontal cortex areas supporting contextual aspects of episodic memory, whereas spindle-ripples can phase-lock with spindles in parietal areas supporting detailed autobiographical recollection. Here, we found that hippocampal sharpwave-ripples preceded cortical ripples by ~250ms (Fig.5F), whereas spindle-ripples were concurrent (Fig.5G), reinforcing a previous suggestion that they make sequential contributions to consolidation[12]. Interestingly, given the anatomical location of the hippocampus at the apex of the cortical hierararchy[28], NREM hippocampal ripples were slightly more likely to co-occur with ripples in early cortical areas as indexed by myelination (SFig.7).

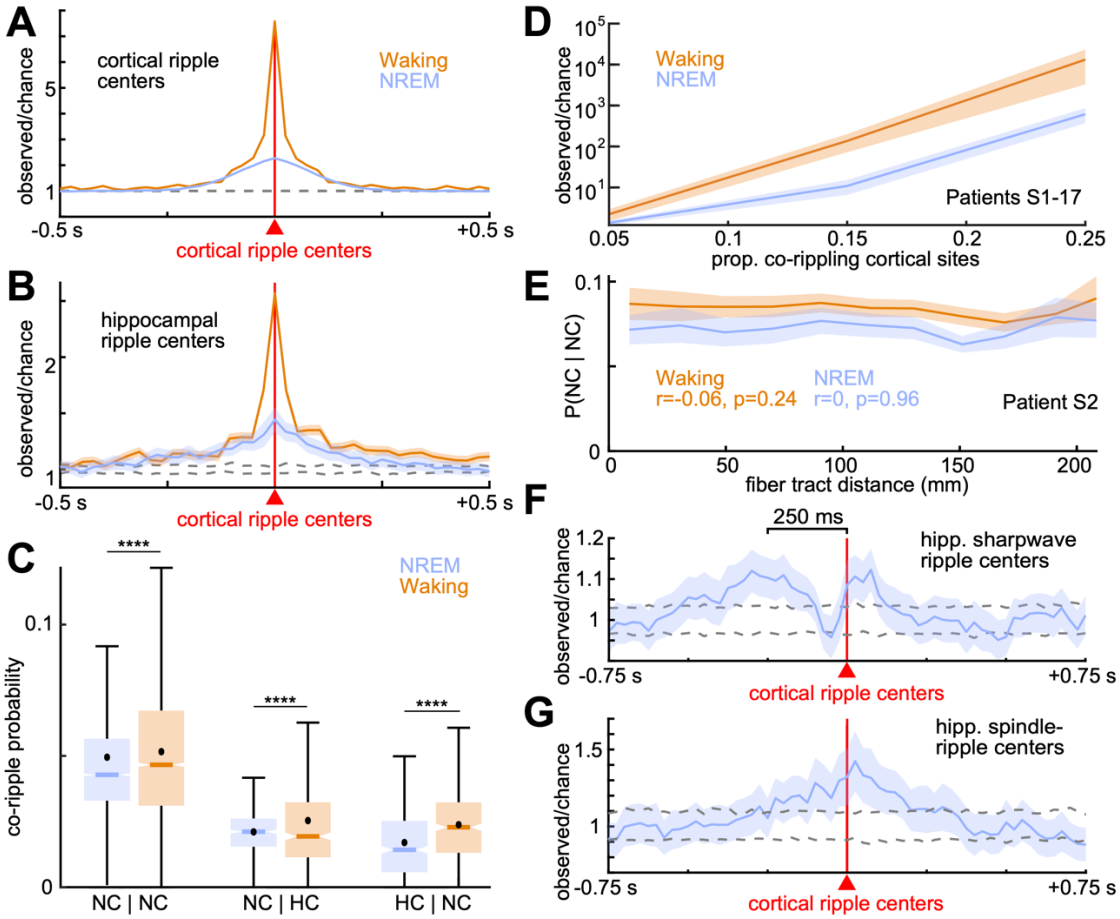

Fig. 5. Cortico-cortical and hippocampo-cortical ripples co-occur during waking and NREM sleep. (**A**) Cortico-cortical ripple time delays between coupled (occurring within 500ms of each other without necessarily overlapping) sites during NREM sleep (*N*=4487/4550 significant

channel pairs) and waking (*N*=4478/4550; post-FDR $p<0.05$, randomization test). Dashed lines show 99% confidence interval of the null distribution (200 shuffles/channel pair). (**B**) Same as (A) except hippocampal ripples relative to cortical ripples (NREM: *N*=133/461; waking: *N*=401/461). (**C**) Conditional co-occurrence probabilities of cortico-cortical and hippocampo-cortical ripples overlapping for at least 25ms (i.e., probability of a ripple in a particular channel given a ripple in another particular channel). (**D**) Observed over chance cortical ripple co-occurrence according to the number of sites co-rippling. (**E**) Cortical ripple co-occurrence probabilities vs. intervening fiber tract distance. (**F-G**) Same as (B) except for hippocampal sharpwave-ripples (*N*=91/461) **(F**) and spindle-ripples (*N*=56/461) (**G**) relative to cortical ripples during NREM sleep. Error shows SEM. ****post-FDR $p<0.0001$, two-sided paired *t*-test.

Cortico-cortical/hippocampal ripple co-occurrence precedes successful recall

To test if cortical ripple co-occurrence was involved in memory recall, we analyzed paired-associates memory task data from 5 SEEG patients (Fig.6A, STables 1,13). Preceding delayed cued recall, there was a significant increase in cortical ripple occurrence ($p=1\times10^{-11}$), and an even greater increase in cortico-cortical ripple co-occurrence ($p=0.0004$, linear mixed-effects; Fig.6B-E). Furthermore, cortical ripple occurrence ($p=0.002$) and cortico-cortical ($p=0.002$) and hippocampo-cortical ($p=0.008$) ripple co-occurrence modulations were greater preceding delayed vs. immediate recall, which shared the same stimuli and responses. Finally, cortico-cortical ($p=0.04$) and hippocampo-cortical ($p=0.004$) co-rippling was enhanced preceding successful vs. unsuccessful delayed recall, which was not the case for cortical ($p=0.08$) or hippocampal ($p=0.94$) ripples generally. These data suggest that ripple co-occurrence between cortical sites and between hippocampus and cortex supports long-term memory recall in humans.

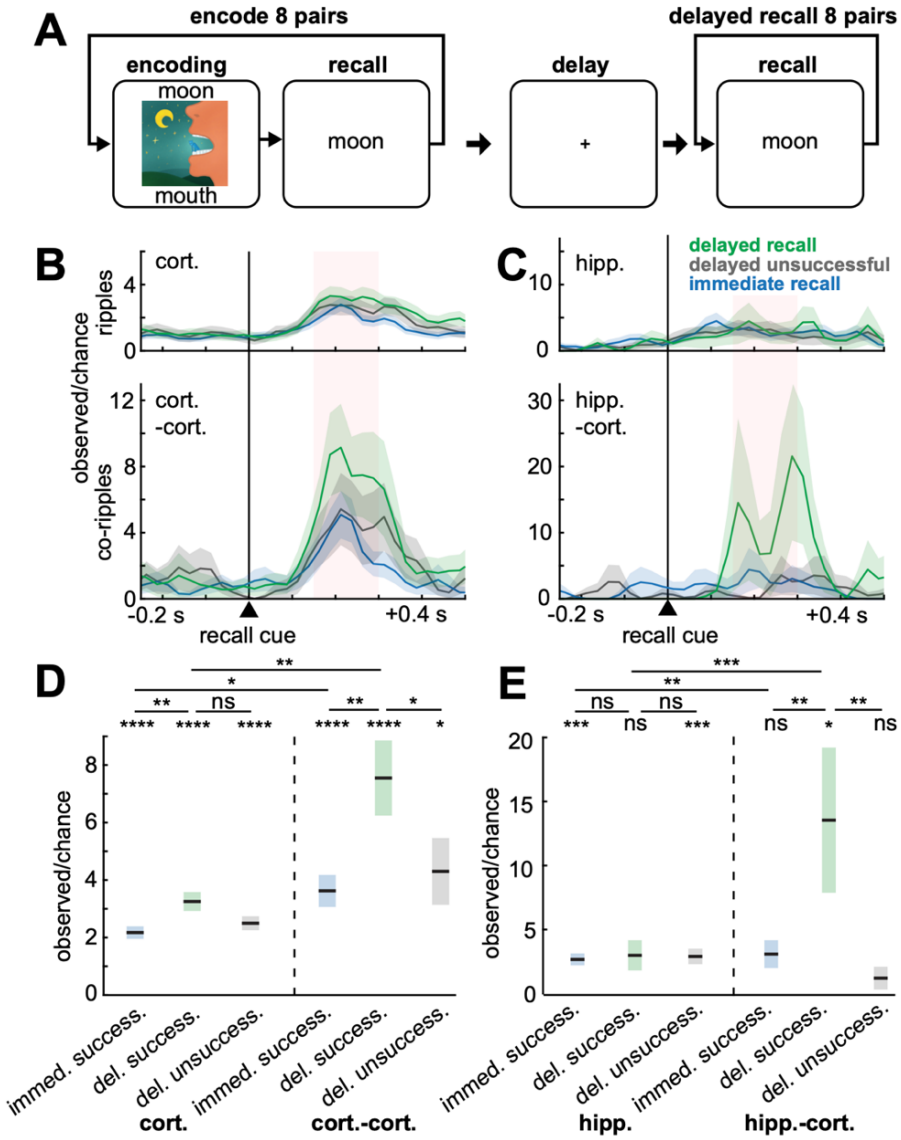

Fig. 6. Cortico-cortical and hippocampo-cortical ripple co-occurrence precedes memory recall. (**A**) Schematic of paired-associates memory task. Patients learned word pair associations and were subsequently cued with the first word to recall the second immediately following learning and then after a ~60s delay. (**B**) Cortical and cortico-cortical co-ripples following stimulus cue preceding successful immediate or delayed recall or unsuccessful delayed recall (delayed *N*=365 trials, immediate *N*=698 trials, patients S18-22). (**C**) Same as (B) except for hippocampal ripples and hippocampo-cortical co-ripples (delayed *N*=90 trials, immediate *N*=304 trials, patients S19,22). **(D**) Quantification of (B) during the shaded 150-300ms interval following stimulus cue onset preceding successful recall in the immediate or delayed condition, or unsuccessful recall (no attempt or incorrect response) in the delayed condition. (**E**) Same as (D) except for hippocampal ripples and co-occurring hippocampo-cortical ripples. Errors show SEM. Post-FDR **p*<0.05, ***p*<0.01, ****p*<0.001, *****p*<0.0001, linear mixed-effects models.

Cortical ripples phase-lock across widespread regions

The precise timing of cortico-cortical communication between sites by oscillations has been hypothesized to underly integration of different components of events across sites ('binding'), originally suggested by inter-hemispheric phase-locking of visually-evoked gamma in cats[29]. We measured phase-locking as the consistency of phase between each pair of sites, across all of their co-ripple events. We found significant phase-locking values[30] (PLV; consistency of 70-100Hz phase, independent of amplitude) of co-occurring ripples between all sampled cortical regions, including between hemispheres, more frequently during NREM sleep than waking (Fig.7A-C, STable 14; post-FDR $p<0.05$, randomization test; non-significant results in SFig.8A-B). During waking, co-ripple phase-lags between channels that had significant co-ripple phase-locking tended to be ~0 or ~π, whereas in NREM sleep phase-lags were often non-zero (Fig.7D). Like ripple co-occurrences, PLV modulations were not associated with distance (Fig.7E, SFig.9, STable 12).

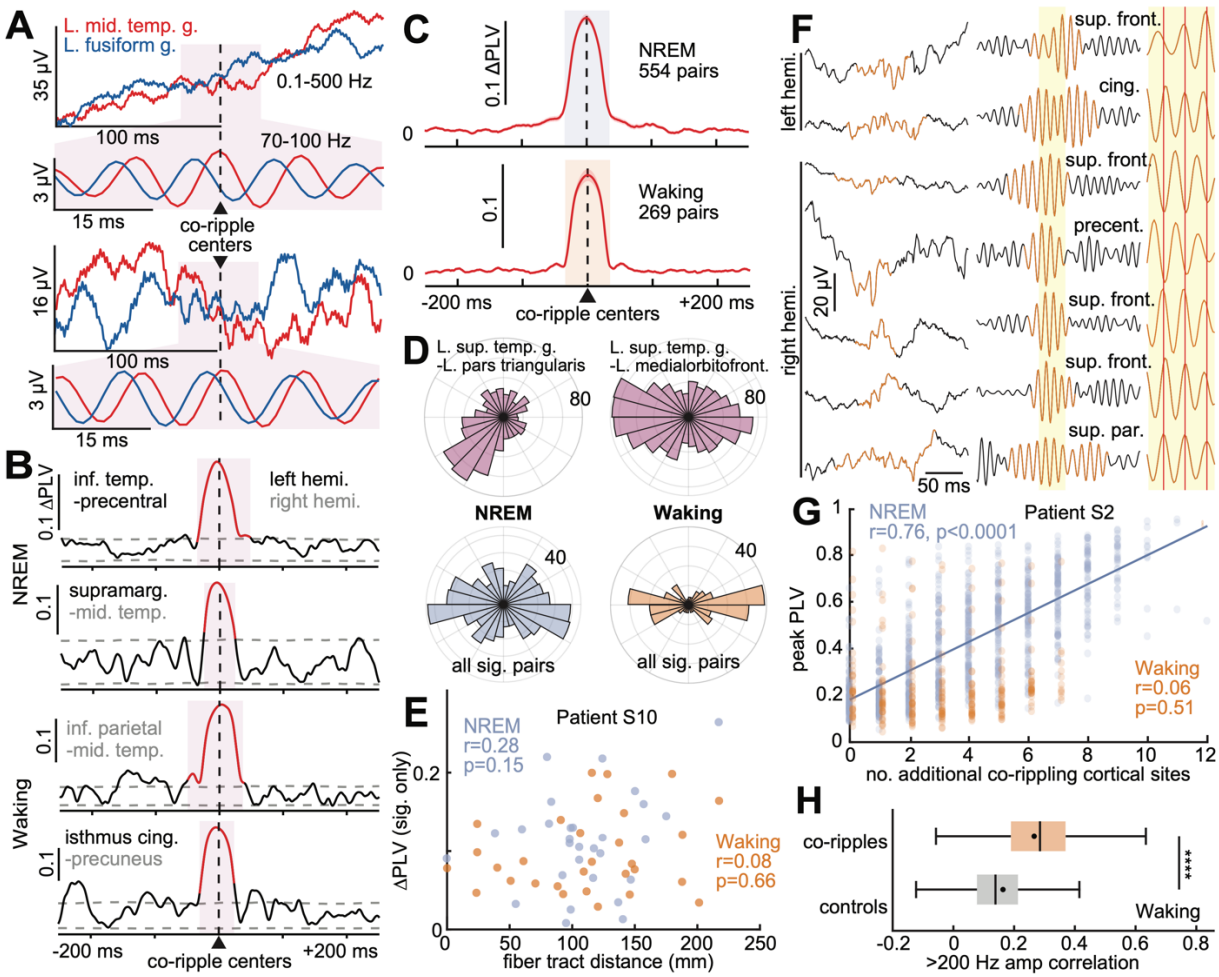

Fig. 7. Ripples synchronize across wide separations in the cortex. (**A**) Two individual ripples in broadband LFP and 70-100Hz bandpass. (**B**) Example 70-100Hz PLV time-courses calculated between ripples co-occurring between ipsilateral and contralateral cortical sites (≥25ms overlap) in NREM sleep and waking. Red shows significant modulation (post-FDR $p<0.05$, randomization test, 200 shuffles/channel pair). (**C**) Average ΔPLVs (relative to -500 to -250ms) for cortical channel pairs with significant PLV modulations. (**D**) Polar histograms of waking and NREM sleep phase-lags across co-ripples for two cortico-cortical pairs with

significant PLV modulations (top) and across channel pair circular means (bottom). Cortico-cortical phase-lags had a significant preference for ~0 or ~π during waking compared to NREM sleep based on the counts within 0±π/6 or π±π/6 vs. outside for NREM sleep vs. waking (p=5×10^{-8}, χ^2=29.75, df=1). (**E**) ∆PLV vs. intervening fiber tract distance for significant pairs. (**F**) Single sweep broadband (left) and normalized 70-100Hz bandpass (right) show ripples (orange) co-occurring across multiple cortical sites during waking. (**G**) Peak PLV as a function of the number of additional cortical sites co-rippling (NREM: N=10/17 patients significant; Waking: N=3/17, post-FDR p<0.05, significance of the correlation coefficient). (**H**) Correlation of the >200Hz analytic amplitude during waking co-ripples compared to randomly selected preceding control periods (within -10 to -2 s) matched in number and duration (N=2275 channel pairs). ****p<0.0001, two-sided paired t-test. PLV=phase-locking value.

Phase-locking increases with more cortical sites co-rippling

Ripples often phase-locked across multiple sites (Fig.7F,G). Widespread co-occurrence and phase-locking of cortical ripples could theoretically arise from a common hippocampal input. However, hippocampo-cortical pairs with co-occurring ripples were seldomly phase-locked (NREM: N=4/277 channel pairs; Waking: N=1/333; SFig.8C-F, STable 14), whereas cortico-cortical co-occurring ripples often were (NREM: N=554/2106; Waking: N=269/1939), a ~20-45 fold difference. This is more consistent with coupled cortical oscillators, as is the strong positive correlation between cortico-cortical phase-locking and the number of sites co-rippling (Fig.7G). These results were consistent when instead using the difference in PLV (e.g., from baseline to peak), which accounts for changes in the baseline, to the number of additional sites co-occurring (N=7/17 patients significant during NREM sleep, 1/17 significant during waking, post-FDR p<0.05, significance of the correlation coefficient). In sum, we have found widespread state-dependent networks of phase-locked 80Hz oscillations over large areas of the cortex.

Co-rippling increases putative unit-activity correlation between distant cortical sites

A putative neurophysiological sign of increased integration across co-rippling locations is increased correlation of multi-unit activity[29]. We used >200Hz amplitude as a proxy for unit-firing[19]. During waking but not NREM, this measure was highly correlated when cortical sites were co-rippling vs. when they were not (Fig.7H, p=8×10^{-303}, two-sided paired t-test). Correlation between co-rippling sites did not significantly decrement with increasing distance between the sites (SFig.10).

As described above, co-ripple phase-lags between channels tended to be near 0 or π. This could indicate that co-rippling sometimes represents a state of inhibited communication, or simply that our bipolar SEEG derivations had variable relationships to local ripple generating dipoles. To test this hypothesis, we compared the >200Hz amplitude correlations between sites, when the sites had co-ripple phase-lags of 0±π/6 vs. π±π/6 (averaged within these ranges for each channel-pair). No significant difference was found for waking or NREM (Waking: p=0.17; NREM: p=0.07, two-sided paired t-test, N=2275 channel pairs), thus supporting the latter explanation.

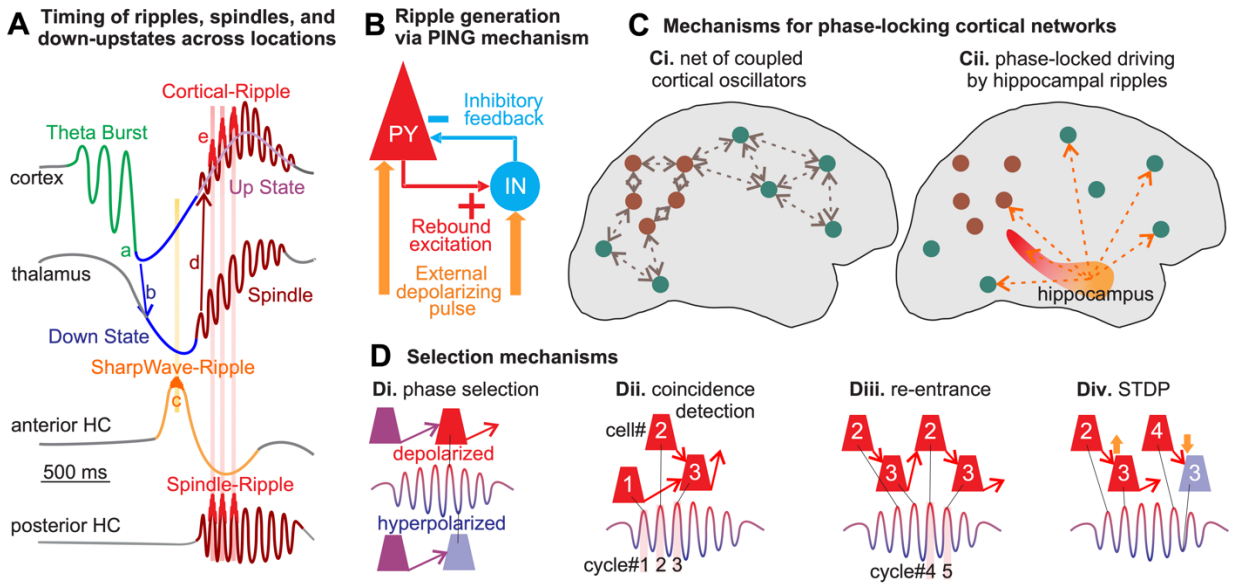

Fig. 8. Cortical ripple integration with sleep waves and proposed mechanisms for generation, phase-locking, and network selection. (**A**) Timing of ripples, spindles, and down-upstates across structures. A cortical theta burst leads to a downstate[21] (*a*) which triggers a thalamic-downstate (*b*) and rebound hippocampal sharpwave-ripple[11] (c) arriving at the cortex rebooting from its downstate; meanwhile, the thalamic-downstate enables h and T currents to generate a spindle projected to the cortex[22] (*d*) with phase-locked posterior hippocampal spindle-ripples[12]. Overall, cortical ripples during NREM follow hippocampal, and occur on the down-upstate slope (e*)*. (**B**) Pyramidal Interneuron Network Gamma (PING) ripple generation mechanism consistent with single-unit recordings (Fig.3E-H), animal studies[31], and modelling[32]. Abrupt depolarization causes synchronous pyramidal (PY) and interneuronal (IN) firing, which then spike rhythmically separated by fixed intervals due to recurrent inhibition. (**C**) Potential mechanisms for ripple phase-locking across broad cortical regions: (**Ci**) direct connections between the cortical oscillators; (**Cii**) distributed driving oscillations from a subcortical location (e.g., hippocampal ripples). (**D**) Multiple synergistic mechanisms enabled by cortico-cortical co-rippling could select a spatiotemporal neural network. Spikes arriving at the depolarized phase (**Di**) or simultaneously from two phase-locked sources are more likely to trigger an action-potential (**Dii**). Re-entrant activation could also result if all three sites are phase-locked (**Diii**), and the synapses effectively evoking spikes would be strengthened with STDP (**Div**).

Discussion

Ubiquity and consistency of ripples across cortical areas, hippocampus and cortex, states (NREM sleep and waking), and species

The current study provides the first comprehensive description of cortical ripples. Using intracranial recordings in humans, we report that cortical ripples are widespread during NREM sleep in addition to waking. Basic ripple characteristics (occurrence density, amplitude, oscillation frequency, duration) are very similar in cortex vs. hippocampus, and NREM vs. waking.

In contrast to the similarity of basic properties, we found that ripples in waking vs. NREM occur within much different immediate physiological contexts. In NREM, cortical ripples are strongly associated with local upstates, downstates, and sleep spindles (Fig.8A). Characteristically,

ripples occur on the upslope ~100ms before the peak of the upstate. Previous studies found that sleep spindles[24] and upstates[23] are associated with strong increases in local unit-firing, and we found that also to be the case for NREM cortical ripples. Similarly, NREM hippocampal ripples in previous studies were found to often occur during local sharp-waves or spindles[10-13]. In contrast, in waking, we found no consistent lower-frequency LFP wave associated with ripples. However, both cortical and hippocampal ripples occurred during greatly increased local >200Hz amplitude, a surrogate for unit-firing[19]. Thus, the local contexts of both cortical and hippocampal ripples, in both NREM and waking, are sudden increases in local excitability lasting ~70ms. NREM and waking are different in that the depolarizing pulse is organized by endogenous sleep rhythms in NREM, but appears to be related to exogenous input, such as a retrieval cue, during waking.

Computational neural models and experimental studies have found that depolarizing pulses can induce oscillations from ~20-160Hz[2,32]. Depolarization causes synchronous pyramidal cell firing, which is inhibited for a fixed time by recurrent inhibition from local basket cells. The pyramidal cells then fire again, resulting in Pyramidal Interneuron Network Gamma (PING) (Fig.8B). As predicted by this model, we found strong ripple phase-modulation of putative pyramidal and interneuronal firing, with pyramids regularly preceding interneurons. Our findings are also consistent with PING supplemented by synchronized basket cell firing and mutual inhibition (ING; Interneuron Network Gamma).[33] Definitive mechanistic demonstration would require experiments not possible *in vivo* in humans[31].

Overall, the characteristics of human ripples enumerated above are similar to those of rodents with one exception: the center frequency of human ripples is ~80Hz[11], whereas in rodents it is ~130Hz[2]. Conceivably, the larger human brain may require more time for cortico-cortical and hippocampo-cortical integration than in rodents.

Cortical ripples and memory (consolidation and recall)

A critical aspect of hippocampal-dependent declarative memories is the linkage of novel constellations of elements encoded in widespread cortical locations. Thus, for replay to facilitate consolidation, it must re-activate spatiotemporal patterns distributed across the cortex. Previously, we showed that widespread spatiotemporal high gamma patterns from waking recur during subsequent NREM[27]. Here, we found that they are tightly coupled with cortical ripples, consistent with ripples having a role in recurrence and potentially replay. Consolidation requires plasticity as well as replay to increase the strength of the connections embodying the memory. The prime candidate is STDP, which occurs when pre- and post-synaptic cells fire in close temporal proximity[34]. We show that local neurons are much more likely to fire at delays optimal for STDP during ripples than control periods. A similar increase is also observed during sleep spindles and upstates in humans[24]. Since NREM cortical ripples are temporally coordinated with sleep spindles and upstates, there is the possibility for a synergistic facilitation of plasticity.

In addition to consolidation during sleep, the hippocampus contributes to recall in the absence of sleep or even quiet rest, and this is striking in transient global amnesia[35]. Indeed, we found that spontaneous hippocampal ripples were just as dense, and more tightly coupled with cortical ripples in waking compared to NREM. However, unlike NREM, during which 67% of hippocampo-cortical channel-pairs with a significant order preference had hippocampal ripples preceding cortical, during waking the opposite was true, with cortex leading in 85%. These observations are consistent with hippocampal ripples during waking contributing to the formation of memories through cortex leading hippocampus, but instead hippocampus leading cortex supporting recall of recent events during waking and replay during consolidation in NREM.

Previous work showed that coupling of anterolateral temporal and parahippocampal ripples in humans increases prior to correct recall in paired-associates learning[16]. We show that such coupling also occurs between hippocampal and cortical ripples. Further, we show that immediate recall with no intervening distractor, a task with identical sensory and motor stimulation but that does not require the hippocampus, is not associated with increased hippocampo-cortical ripple coupling. Critically, given the importance of transcortical connections in declarative memory, we show that cortico-cortical ripple coupling also strongly increases prior to correct recall following a delay.

During NREM, hippocampal ripples mark the local replay of spatiotemporal patterns of hippocampal neuronal firing, hypothesized to be transmitted cortically to guide cortical replay and consequently consolidation. Consistent with this hypothesis, we found that hippocampal and cortical ripples were often coupled in time during NREM, with cortical following hippocampal ripples. During NREM, many hippocampal ripples, especially in anterior hippocampus, occur at the peak of the sharpwave[11], and in the posterior hippocampus, ~200ms later at peaks of the local spindle[12] (Fig.8A). We found that hippocampal sharpwave-ripples tend to precede cortical ripples coinciding with hippocampal spindle-ripples by ~250ms. Sharpwave-ripples are more associated with sleep waves in prefrontal cortex areas supporting contextual aspects of episodic memory[11], whereas spindle-ripples can phase-lock with spindles in parietal areas supporting detailed autobiographical recollection[12]. The current results provide further evidence of a prolonged distributed hippocampo-cortical interaction during consolidation.

Coordination of cortical ripples with ripples in other cortical sites and the hippocampus

A novel finding of this study is that spontaneous cortical ripples couple (within ±500ms), co-occur (≥25ms overlap), and often phase-lock across large areas of both hemispheres during both sleep and waking. The lack of a decrement with distance in co-occurrence or phase-locking suggests either a central driving oscillator, or a population origin, such as a web of coupled oscillators (Fig.8C). The hippocampus is unlikely to act as a central driving oscillator because hippocampo-cortical coupling and co-rippling is rarer than cortico-cortical, and hippocampo-cortical phase-locking is essentially absent. The preponderance of cortico-cortical influences might be expected given that each cortical pyramidal cell receives input from thousands of other pyramids, whereas the fan-out from hippocampus (CA1 plus subiculum) to cortex is ~1:500, so each cortical pyramid gets on average less than 10 hippocampal synapses[36,37]. Conversely, a network of coupled oscillators is consistent with the strong positive feedback we observed in the spread of cortico-cortical co-occurrence and intensity of cortico-cortical phase-locking. Specifically, cortico-cortical co-occurrence probability during waking increases from ~2x chance levels for 2 sites to ~20,000x chance for 25% of the sites. Similarly, during NREM, peak cortical ripple PLV between sites increases monotonically with the number of additional sites co-rippling, from ~0.2 with no additional sites to ~0.9 with twelve. Modelling studies show that phase-locked oscillations at 80Hz can occur in extended cortical networks, even at zero lag, provided that the neurons have multiple-path recurrent connectivity[25,38].

We found that cortico-cortical co-rippling and phase-locking show consistent differences between states. Although spontaneous cortical ripple occurrence density is higher in NREM, co-occurrence density is higher in waking. Accordingly, the likelihood of multiple sites co-rippling relative to chance grows more rapidly with number of sites during waking than NREM, the increase being ~25x larger when 25% of sites are co-rippling. The proportion of ripple peaks that occur within 25ms of each other is ~5x greater in waking than NREM. Furthermore, when co-ripples phase-lock they are more likely to be effectively synchronous in waking than NREM.

These properties are consistent with a rapid highly synchronous recruitment of multiple cortical sites by a high activation during waking ripples. Higher activation is indicated by the ~10x higher increase in >200Hz amplitude during waking vs. NREM ripples. Conversely, NREM ripples tend to recruit sequentially across the cortex, with a smaller but significant increase in both >200Hz amplitude and in associated cell-firing.

A mean of about 16 widely-distributed cortical locations were sampled per patient. Assuming that a ripple generating module spans ~1mm^2 of cortical surface (unpublished data), this indicates that we recorded from only ~1/10000th of the ripple modules. However, the lack of relation of co-rippling to distance indicates that the spacing between cortical recording sites exceeds the size of ripple modules, and allows the proportion of recorded sites to be used as an estimate of the proportion of the cortex that is rippling. If so, then at times, as much as 25% of the cortex is co-rippling. Similarly, the usual proportion of the cortex co-rippling can be roughly estimated from the probability, given a ripple, that another site is co-rippling, ~8% (assuming that the ripple's lead-field is comparable to its module size).

Given the strong ripple phase-modulation of cell-firing we demonstrated, ripples can be expected to strongly modulate the effectiveness of arriving synaptic input, with spikes arriving on the depolarized phase being far more likely to trigger post-synaptic firing. Thus, there may be a strong selection for cells that project (even multi-synaptically) between co-rippling sites with a latency matching the phase-lag (possibly plus multiples of the cycle time, Fig.8Di). Additionally, when multiple sites co-ripple, then spikes that arrive together at a third location may have greatly enhanced effectiveness (i.e., the post-synaptic site acts as a coincidence detector) (Fig.8Dii)[39]. Synaptic phase-selection and coincidence detection are synergistic, and would further imply positive feedback due to recurrence (Fig.8Diii), and be progressive because the pre- and post-synaptic activation these mechanisms would strengthen in-phase connections via STDP (Fig.8Div). Note that these mechanisms would also function between sites that are co-rippling but not phase-locked according to our criteria, which required consistency of phase-lags across all waking or NREM co-ripples of a site-pair. Even without such a pattern, selection would occur because phase is generally consistent within each co-ripple due to the small range of ripple frequencies (50% within ~0.3Hz of the mean). Thus, through gain modulation and coincidence detection[29], co-rippling may strongly select the distributed cortical network active during a co-rippling event. Some indication that this may be the case was our finding that >200Hz amplitude has a higher correlation between locations when they are co-rippling.

Through these mechanisms, cortical ripples could activate and couple with distant but related encoders through progressive activation of a web of cortico-cortical positive feedback connections. The strongly increased probability of co-activation and phase-locking with increasing numbers of contacts already co-activating suggests positive feedback recruitment of the most interconnected and co-activated cells into a brief synchronous ripple. When locations join the rippling network and resonate with other members, their activity level increases. The function of the ripple could thus be to act as an amplifier through resonance, leading to the rapid assembly of a network encoding the various aspects of an event.

Binding

The Binding Problem asks 'How are the various contents of a mental event united into a single experience?' For example, how different visual qualities of an object (e.g., color, shape, location, motion, texture) are associated with each other[40], or more generally how sensations in different modalities, feelings, and thoughts are combined in a single experience[41]. One prominent theory proposes that binding occurs through temporal synchrony in the gamma

range[29]. Experimental evidence for such synchrony is typically (but not always) at short distances, at 30-40Hz, in early visual cortex of cats to particular simple visual stimuli[41]. Since the cross-cortical integration function proposed for ripples in the current study may be considered a form of binding, their ubiquity may help address some critiques of the binding-by-coherence model[42,43]. First, ripples occur in all regions of the cortex in both hemispheres (required by binding because the elements of experience are encoded throughout the cortex). Second, ripples occur spontaneously throughout waking and NREM sleep (required since binding is a ubiquitous process), and are elevated during task periods when binding may be useful (such as reassembling the components of a memory). Third, ripples last ~70ms, a duration considered in the range of 'the psychological moment.' Fourth, ripples strongly increase local firing and firing-proxy >200Hz amplitude (required because encoding is associated with activation). Fifth, ripples strongly phase-modulate local putative pyramidal and interneuron firing in a manner consistent with input modulation (a primary hypothesized mechanism whereby oscillations selectively amplify particular neural assemblies). Sixth, ripples strongly co-occur and phase-lock between cortical sites indicating active cortico-cortical communication (required because without communication there cannot be integration). This strong phase-locking occurs between cortical sites but not between cortex and hippocampus, indicating that trans-cortical synchrony is probably intrinsic, i.e., not projected from elsewhere. Furthermore, co-occurrence and phase-locking is minimally affected by distance (required for integration of diverse elements). Finally, >200Hz amplitude is more correlated between sites when they are co-rippling, further suggesting interareal integration of unit-firing.

The principle alternative proposed mechanism for binding relies on hierarchical convergence in multi-attribute, multisensory areas[42,43]. This mechanism seems inconsistent with the highly distributed nature of cortical processing, and poses the difficulty how to pre-represent in a small cortical module each of the combinatorial possibilities of all elements contained in all potential experiences. However, the hippocampus seems to do this, albeit temporarily, with receptive fields that combine indicators of position from multiple modalities, as well as valence, history, and context[44].Hippocampal assembly of the different elements of an event does not require integration across the hippocampus because these elements are available locally, having been pre-mixed by the entorhinal cortex and dentate gyrus. Thus, hippocampal ripples are for communication with the cortex rather than with other hippocampal sites, and indeed they are typically local within the hippocampus[12,45]; rather, their crucial co-occurrences may be with widespread cortical ripples. In this view, binding of cortical elements can occur in the absence of hippocampal input if they are previously consolidated, because cortico-cortical co-rippling and phase-locking is dependent on intracortical processes. Although speculative, these possibilities may merit consideration as potentially enabled by the distributed network of cortical oscillations revealed by the current study.

Methods

Patient selection

Data from a total of 26 patients (14 female, 32±12 years old) with pharmaco-resistant epilepsy undergoing intracranial recording for seizure onset localization preceding surgical treatment were included in this study (STables 1, 6, 8). Patients whose stereoelectro-encephalography (SEEG) recordings were analyzed were only included in the study if they had no prior brain surgery; background EEG (with the exception of epileptiform transients) in the normal range; and electrodes implanted in what was eventually found to be non-lesional, non-epileptogenic cortex, as well as non-lesional, non-epileptogenic hippocampus (such areas were suspected to

be part of the focus prior to implantation, or were necessary to pass through to reach suspected epileptogenic areas). In 3 of these patients, previously collected electrocorticography (ECoG; subdural grids and strips) recordings were analyzed.

Furthermore, 3 of these patients undergoing electrocorticography and SEEG recording for the clinical purpose of seizure localization were also implanted with an intracranial microelectrode (Utah Array) into tissue that was suspected based on pre-surgical evaluation to be included within the region of the therapeutic resection. The implantation of the array did not affect clinical monitoring. In every case it was later resected in order to gain access to the surgical focus beneath. In all of these patients the electrode was determined not to be implanted in an epileptogenic zone and no seizures originated from the region of the array in any of the patients.

Patients were excluded from the study if they had prior brain surgery or did not have non-lesioned hippocampal and cortical channels that were not involved in the early stage of the seizure discharge and did not have frequent interictal activity or abnormal local field potentials. Based on these criteria, 26 were included in this study out of a total of 89. All patients gave fully informed written consent for their data to be used for research as monitored by the local Institutional Review Boards at Cleveland Clinic, Partners HealthCare (including Massachusetts General Hospital), University of California, San Diego, and Oregon Health & Sciences University,

Intracranial recordings

Patients were implanted with intracranial electrodes for ~7 days with continuous recordings for seizure onset localization. SEEG and ECoG electrode implantation and targeting were made for purely clinical purposes. SEEG recordings (*N*=17 patients) were collected with a Nihon Kohden JE-120 amplifier at 1000Hz sampling (patients S1-17), Natus Quantum LTM amplifier at 1024Hz (patients S18-19), or Natus Xltek EMU128FS (patients S20-22). Standard clinical electrodes were 0.8mm diameter, with 10-16 2mm long contacts at 3.5-5mm pitch (~150 contacts/patient). In addition, patients S19 and S22 had electrodes with 0.5-2mm long contacts at 1-2mm pitch. ECoG recordings were collected at 500Hz (patient E1) or 512Hz (patients E2-3) using 128-channel clinical cable telemetry systems (STable 8).

Microelectrode recordings from 3 patients implanted with a Utah Array were also analyzed (STable 6). The Utah Array is a 10x10 microelectrode array with corners omitted and 400µm contact pitch[46-48]. Each silicon probe is 1 or 1.5mm long with a base of 35-75µm that tapers to 3-5µm. The probes are insulated except for the platinum-coated tip. Data were acquired at 30kHz (Blackrock Microsystems) with a 0.3-7.5kHz bandpass. Data were referenced with respect to a distant reference wire. SFig.3A shows the ripple average local field potential (LFP), time-frequency, and a single trial example for a representative channel.

Electrophysiology pre-processing

Offline data preprocessing was performed in MATLAB 2019b and LFPs were inspected visually using the FieldTrip toolbox[49]. SEEG data were downsampled to 1000Hz with anti-aliasing and 60Hz notch filtered (zero-phase) with 60Hz harmonics up to 480 Hz. Transcortical contact pairs were identified using both anatomical location (using the pre-operative MRI aligned to the post-operative CT), and physiological properties (high amplitude, coherence and inversion of spontaneous activity between contacts), and selected such that no 2 pairs shared a contact, with the exception of the 1mm spaced hippocampal bipolar channels described above. All

SEEG analyses were done using bipolar derivations between contacts separated by 1-5 mm in cortical or hippocampal gray matter in order to ensure that activity was locally generated[50].

Channel selection

Channels were excluded from analysis if they were in lesioned tissue, involved in the early stages of the seizure discharge, had frequent interictal activity, or abnormal local field potentials. From the total 2772 bipolar channels (1326 left hemisphere) in the 22 SEEG patients (S1-22), 52 hippocampal (24 left hemisphere) and 403 transcortical (180 left hemisphere) bipolar channels were selected for the analyses (STable 1). Polarity was corrected for individual bipolar channels such that downstates were negative and upstates were positive. This was accomplished by ensuring that during NREM sleep negative peaks were associated with decreased and positive peaks were associated with increased mean ±100ms 70-190Hz analytic amplitude, an index of cell-firing that is strongly modulated by downstates and upstates[23].

Electrode localization

Cortical surfaces were reconstructed from the pre-operative whole-head T1-weighted structural MR volume using the standard FreeSurfer recon-all pipeline[51]. Atlas-based automated parcellation[52] was used to assign anatomical labels to regions of the cortical surface in the Destrieux[53] atlas. In addition, automated segmentation was used to assign anatomical labels to each voxel of the MR volume, including identifying voxels containing hippocampal subfields [54]. In order to localize the SEEG contacts, the post-implant CT volume was registered to the MR volume, in standardized 1mm isotropic FreeSurfer space, using the general registration module[55] in 3D Slicer[56]. The position of each SEEG contact, in FreeSurfer coordinates, was then determined by manually annotating the centroids of electrode contact visualized in the co-registered CT volume. Each transcortical contact pair was assigned an anatomical parcel from the atlas above by ascertaining the parcel identities of the surface vertex closest to the contact-pair midpoint. Subcortical contacts were assigned an anatomical label corresponding to the plurality of voxel segmentation labels within a 2-voxel radius. Transcortical contact pair locations were registered to the fsaverage template brain for visualization by spherical morphing[57]. To plot values on a template brain, channel means were averaged for each cortical region (with the two hemispheres combined) and then morphed onto a left hemisphere ico5 fsaverage template. White-matter streamline distances between channels were computed using the 360 parcels of the HCP-MMP1.0 atlas[58], as determined by probabilistic diffusion MRI tractography[59], are population averages from[20]. When two channels were in the same HCP parcel the distance was considered to be 0. Cortical regions otherwise described in this study are amalgamations of the Desikan parcels[60] as specified in STable 15.

Time-frequency analyses

Average time-frequency plots of the ripple event-related spectral power (ERSP) were generated from the broadband LFP using EEGLAB[61]. Event-related spectral power was calculated from 1Hz to the Nyquist frequency (500Hz except for 250Hz in patient E1 and 256Hz in E2-3) with 1Hz resolution with ripple centers at t=0 by computing and averaging fast Fourier transforms with Hanning window tapering. Each 1Hz bin of the time-frequency matrix was normalized with respect to the mean power at -2000 to -1500ms and masked with two-tailed bootstrapped significance (N=200) with FDR correction and α=0.05 using -2000 to -1500ms as baseline.

Sleep and waking epoch selection

Epochs included in the study did not fall within at least 1 hour of a seizure and were not contaminated with frequent interictal spikes or artifacts. NREM sleep periods were selected from continuous overnight recordings where the delta (0.5-2Hz) analytic amplitude from the cortical channels was persistently increased (STable 1). Sleep epochs were confirmed by visual inspection to have normal appearing spindles, downstates, and upstates, with expected densities, amplitudes, and frequencies (STable 4). Waking periods were selected from continuous daytime recordings that had persistently low cortical delta as well as high cortical alpha (8-12 Hz), beta (20-40Hz), and high gamma (70-190Hz) analytic amplitudes. When the data included electrooculography (EOG; *N*=15/17 SEEG patients), waking periods also required that the 0.5-40Hz analytic amplitude of the EOG trace was increased. Waking epochs were required to be separated from periods of increased delta analytic amplitude by at least 30 minutes.

Ripple detection

The median center frequency of hippocampal ripples in 9 studies was ~85Hz in humans[10,12,16,18,62-66], whereas in rodents, sharpwave-ripple frequency is ~120-140Hz. In humans, putative 80Hz hippocampal ripples have the same characteristic relation to sharpwaves, intra-hippocampal localization, modulation by sleep stage, and relation to cortical sleep waves as in rodents, and occur in hippocampi that have no signs of epileptic involvement. Furthermore, in rodent hippocampus the distinction between higher frequency gamma bursts and ripples is not always sharp, leading to the suggestion that for simplicity they both be referred to as 'ripples'[31], which we follow here.

Ripple detection was performed in the same way for all structures and states and was based on a previously described hippocampal ripple detection method[11,12]. Requirements for inclusion and criteria for rejection were determined using an iterative process across patients, structures, and states. Data were bandpassed at 60-120Hz and the top 20% of 20ms moving root-mean-squared peaks were detected. It was further required that the maximum z-score of the analytic amplitude of the 70-100Hz bandpass was greater than 3 and that there were at least 3 distinct oscillation cycles in the 120Hz lowpassed signal, determined by shifting a 40ms window in increments of 5ms across ±50ms relative to the ripple midpoint and requiring that at least 1 window have at least 3 peaks. Adjacent ripples within 25ms were merged. Ripple centers were determined as the time of the maximum positive peak in the 70-100Hz bandpass. To reject epileptiform activities or artifacts, ripples were excluded if the absolute value of the z-score of the 100Hz highpass exceeded 7 or if they occurred within 2s of a ≥1mV/ms change in the LFP. Ripples were also excluded if they fell within ±500ms of putative interictal spikes, detected as described below. To exclude events that could be coupled across channels due to epileptiform activity, we excluded ripples that coincided with a putative interictal spike on any cortical or hippocampal SEEG or ECoG channel included in the analyses. Events in SEEG and ECoG recordings that had only one prominent cycle or deflection in the broadband LFP that manifested as multiple cycles above detection threshold in the 70-100Hz bandpass were excluded if the largest valley-to-peak or peak-to-valley absolute amplitude in the broadband LFP was 2.5 times greater than the third largest. For each channel, the mean ripple-locked LFP and mean ripple band were visually examined to confirm that there were multiple prominent cycles at ripple frequency (70-100Hz) and the mean time-frequency plot was examined to confirm there was a distinct increase in power within the 70-100Hz band. In addition, multiple individual ripples in the broadband LFP and 70-100Hz bandpass from each channel were visually examined to confirm that there were multiple cycles at ripple frequency without contamination by

artifacts or epileptiform activity. Channels that did not contain ripples that meet these criteria were excluded from the study.

Additional analyses were performed specifically on sharpwave-ripples and spindle-ripples detected according to our previous methods[11,12]. First, NREM sleep data were bandpassed from 70-100Hz, and a putative ripple was detected when the 20ms moving root-mean-squared amplitude exceeded the 90th percentile. Ripples were required to have at least 3 distinct oscillation cycles as described above. Broadband LFP data ±2s around ripple centers underwent 1-D wavelet (Haar and Daubechies) decomposition to detect and remove sharp transients. Ripples were classified as sharpwave-ripples based on the similarity of the peri-ripple LFP to the 400ms average biphasic waveform template created for each subject using 100-300 hand-marked hippocampal sharpwave-ripples, as quantified by the dot product between the template and the peri-ripple LFP (-100 to 300ms), and the absolute difference between the LFP value at the ripple center. Ripples were classified as spindle-ripples if the ripple center occurred during a hippocampal spindle, detected in the same way as described below for cortical spindles, on the same channel. Ripples could be classified as both sharpwave-ripples and spindle-ripples if they met both of these criteria.

Unit detection, classification, quality, and isolation

Unit detection and classification was performed according to our published procedures[24,67-72]. Data were bandpassed at 300-3000Hz and putative unit spikes were detected when the filtered signal exceeded 5 times the estimated standard deviation of the background noise. Units were k-means clustered using the first three principal components of each spike. Overlaid spikes were examined visually and those with abnormal waveforms were excluded. Based on their waveforms, firing rates, and autocorrelograms, action potentials were clustered as arising from putative pyramidal cells or interneurons. Putative pyramidal cells had spike rates of ~0.1-0.8Hz, long valley-to-peak and half width intervals, sharp autocorrelations, and bimodal inter-spike interval (ISI) distributions, reflecting a propensity to fire in bursts (STable 6). By contrast, putative interneurons had spike rates of ~1-5Hz, short valley-to-peak and half width intervals, broad autocorrelations, and a predominantly unimodal ISI distribution.

Single unit quality and isolation were confirmed according to previously established guidelines[73]. Unit spikes were verified to well-exceed the noise floor based on large peak signal-to-noise ratios (SFig.11A). Since the neuronal spiking refractory period is about 3ms, the percent of ISIs less than 3ms estimates the degree of single unit contamination by spikes from different units, which was very low among the units included in this study (SFig.11B). Furthermore, single units detected on the same contact were highly separable according to their projection distances[74] (SFig.11C). Lastly, temporal stability of unit spikes over time was confirmed based on consistency of the mean waveform shape and amplitude of each unit across recording quartiles.

Sleep graphoelement detection

Downstates and upstates were detected as previously described[11,12], where data from each channel were bandpassed from 0.1-4Hz (zero-phase shift) and consecutive zero crossings separated by 0.25-3s were selected. The top 10% amplitude peaks were selected and the polarity of each signal was inverted if needed so that downstates were negative and upstates were positive by confirming that the average analytic amplitude of the 70-190Hz analytic amplitude ±100ms around peaks was greater for upstates than downstates.

Spindles were detected as previously described[75], where data were bandpassed at 10-16Hz, then the absolute values were smoothed via convolution with a tapered 300ms Tukey window, and median values were subtracted from each channel. Data were normalized by the median absolute deviation and spindles were detected when peaks exceeded 1 for at least 400ms. Onsets and offsets were marked when these amplitudes fell below 1. Putative spindles that coincided with large increases in lower (4-8Hz) or higher (18-25Hz) band power were rejected to exclude broadband events as well as theta bursts, which may extend into the lower end of the spindle range[21].

Interictal spike detection and rejection

Ripples and sleep graphoelements were excluded if they were within ±500ms from putative IIS detected as follows. A high frequency score was computed by smoothing the 70-190Hz analytic amplitude with a 20ms boxcar function and a spike template score was generated by computing the cross-covariance with a template interictal spike. The high frequency score was weighted by 13 and the spike score was weighted by 25, and an IIS was detected when these weighted sums exceeded 130. In each patient, detected IIS and intervening epochs were visually examined from hippocampal and cortical channels (when present) to confirm high detection sensitivity and specificity.

Cortical replay analyses

We performed new analyses on data from subjects 2-4 in Jiang et al., (2017)[27] (STable 8). Analyses were performed on "Events" that were sequences of high gamma (70-190Hz) peaks identified during waking that recurred during the following NREM sleep, and which were considered 'exact matches,' such that all common channels had the same temporal order. Events consisting of high gamma peaks were identified as follows: outlier high gamma peaks were counted in 2s windows moving in 50ms increments. Events were identified when windows had local maxima of high gamma outlier peaks (minimum 4). When there were multiple high gamma peaks from the same channel during a given Event, only the median high gamma peak position across these channels was used.

Spatiotemporal Motifs were selected using methods from rat cortical electrophysiology studies. Events were grouped according to spatial distribution similarity in R with the packages Fast Hierarchical Clustering Routine[76] and Dynamic Tree Cut[77] using Phi-coefficient-derived distance matrices[78] and Ward's method[76]. Motifs, which occurred during waking and NREM sleep, were identified by grouping waking Events based on high gamma peak order and then matching them to NREM Events. Temporal order similarity for waking Events in each cluster was computed using the matching index (MI) algorithm, which was implemented as previously described[5], except using high gamma peaks in place of spike train convolutions in MATLAB with custom scripts and in R with the TraMineR toolbox[79], with an additional heuristic criterion that only the channels in common for each comparison were used to calculate MI. This metric of pattern similarity required that each channel had a unique position in the sequence since channel pair orders were compared with the MI.

Each cluster of spatially similar waking Events was subsequently divided into subclusters. Motifs that included 90% of a given subcluster's Events in their neighborhoods, defined as 20% of the maximum distance between two Events for a given subcluster, were selected. These were then matched with MI to the Events in NREM sleep, and each representative was associated with a certain number of replay frames (i.e., NREM Events that matched the waking Motif, or "Motif-Event matches") for each NREM period. If multiple Motifs matched to the same NREM Event

the number of replay frames associated with each waking Motif for that night was incremented by 1/*N* instead of 1, where *N* was the number of waking Motifs matched to the Event. Therefore, the total increments from any given Event was equal to 1 regardless of the number of matching Motifs as long as there was at least one match. The resulting replay frame numbers for each NREM period were then normalized by the total number of Events found in that NREM period. Waking motifs were required to match at least 2 Events.

Counts were made for Motifs that had more Motif-Event matches during the preceding than following NREM sleeps. This was compared to the number with the reverse pattern with a two-sided binomial test with an expected value of 0.5. Motifs were only included if their total number of NREM Event matches across all 4 nights (2 preceding waking, 2 following) exceeded Motif-wise thresholds established by matching preceding sleep and post sleep Event to the same Motifs with the channel order randomly shuffled 1000 times.

Paired-associates memory task

Paired-associates memory task data were collected from 5 patients using Presentation (Neurobehavioral Systems). Patients were instructed to memorize a series of word pairs and to recall the second word when cued with the first. A word pair was presented with text and audio (pre-recorded speech) along with an integrating image that contained semantic content of both words. After each presentation, immediate recall was assessed by cuing the first word immediately after the offset of the word pair and image. The patient then attempted to recall the word aloud. This was repeated with 8 different pairs followed by a 6s break, and then delayed recall of the 8 pairs was assessed in the same order where the first word was cued and the patient attempted to recall the second word aloud. After 4s the integrating image was displayed. Delayed recall was only considered successful if the second word was said aloud before the image appeared. This sequence was repeated 20 times for a total of 160 word pairs. For one patient (S18), the task was instead structured as 25 sets of 6 pairs with the integrating image shown during the encoding period but not during delayed recall, and instead during delayed recall the second word was presented after 5s. Delayed recall was only considered successful for this patient if the second word was said aloud before it was presented after 5s. Task performance by patient is summarized in STable 13.

During the task, audio containing the stimulus presentations and patient voice was split and simultaneously recorded into the task presentation computer and into the clinical amplifier system synchronously with the intracranial recordings. Stimulus markers sent by the task computer were also synchronized with the intracranial recordings. Scoring of behavioral data was done offline by listening, and recall onsets were identified offline using Audacity v2.4.2 through both visual examination of the task computer recorded audio waveforms and spectrograms and confirmation through listening. The computer recorded audio was downsampled with anti-aliasing to 1000Hz and cross-correlated with the audio recorded alongside the intracranial recordings to ensure high temporal precision of recall onsets.

Ripple occurrences and co-occurrences relative to the word cue (text and audio) preceding recall onsets prior to successful (i.e., correct response before the answer or integrating image was presented in the delayed condition) or unsuccessful (i.e., no response, incorrect response, or response after the answer or image was presented) were computed across trials, where each trial was an average across channels. Null distributions of occurrences were computed by randomly shuffling ripple or co-occurring ripple centers for each channel in each trial within ±3s from cue onset 10 times. Observed over chance (average of null) ripple occurrence and co-occurrence histograms had 25ms bins Gaussian-smoothed with a 100ms window. Trial-wise

ripple occurrence and co-occurrence averages in the 150-300ms window following cue onset were computed for statistical analyses.

Analyses of unit spiking during ripples

Unit spiking was analyzed with respect to local ripples detected on the same contact. The percent of baseline spike rate during ripples was computed by multiplying 100 times the spike rate of concatenated ripples divided by the spike rate of concatenated randomly selected epochs in between ripples that were matched in number and duration to the ripples. Ripple phases of unit spikes were determined by finding the angle of the Hilbert transform of the 70-100Hz bandpassed signal (zero phase shift) at the times of the spikes. The circular mean ripple phase was determined for each unit using[80]. Phase analyses were only performed on units that had at least 30 spikes during local ripples. PY-PY and IN-IN unit pair co-firing within 5ms was assessed based on[24]. To evaluate co-firing when there was a ripple at either or both sites vs. baseline when there were no ripples occurring, we randomly selected 200 sets of non-ripple epochs matched in number and duration to the ripples but during which there were no ripples detected on either channel. Co-firing during ripples with observed vs. random spike times was computed by shuffling the spike times of each unit within the intervals of the ripples 200 times.

Ripple temporal relationships

Peri-cortical ripple time histograms of cortical graphoelements or Motif high gamma peaks on the same channel, or of cortical or hippocampal ripples on a different channel (i.e., a channel pair) were computed. Gaussian smoothed (250ms window) event counts were found in 25ms bins for ripples or 50ms for graphoelements within ±1500ms relative to cortical ripple centers at t=0. A null distribution was generated by shuffling the event times relative to the ripples at t=0 within this 3s window 200 times each. Pre-FDR p-values were computed by comparing the observed and null distributions within each bin over ±1000ms for cortical graphoelements or ±500ms for ripples. These p-values were then FDR-corrected for the number of channel (pairs) across patients multiplied by the number of bins per channel (pair)[81]. A channel (pair) was considered to have a significant modulation if there were 3 or more consecutive bins with FDR-corrected p-values less than α=0.05. Whether events were leading or lagging cortical ripples at t=0 was computed for each channel (pair) with a two-sided binomial test with expected value of 0.5, using event counts in the 1000ms before vs. 1000ms after t=0 for graphoelements and 500ms before vs. 500ms after t=0 for ripples. For plots, 50ms Gaussian smoothed event counts with 50ms bins were used.

Conditional probabilities of a ripple given the following graphoelements or their sequences were computed: downstate, spindle, upstate, downstate–spindle, and spindle–upstate. A ripple given a spindle (R | SS) was determined if the ripple center occurred during the spindle (average spindle duration was 634ms). A ripple was considered to precede an upstate or follow a downstate if the ripple center occurred 634ms before or after the peak of the upstate or downstate, respectively.

Cortical ripple co-occurrences

Co-occurring cortical ripples (“co-ripples”) between two cortical channels were determined by finding ripples that overlapped for at least 25ms. The center of the co-occurring ripple event was determined by finding the temporal center of the ripple overlap. Conditional probabilities of ripple co-occurrence were computed by finding the probability of co-occurrence (minimum 25ms overlap) between two channels given that there was a ripple in one of the channels, separately

for each channel. This was done for P(NC|NC) (both orders), P(NC|HC), and P(HC|NC). To estimate the extent of co-rippling across the cortex at any moment, the probability that a given proportion of channels was co-rippling at any time point for each subject was computed. Co-occurrence probability as a function of distance was computed.

Observed over chance cortical ripple co-occurrence was computed as a function of the number of sites co-rippling. Ripple co-occurrence of a given number of sites required that all of those sites had at least 25ms ripple overlap. Chance was computed for each patient by randomly shuffling the ripple epochs and inter-ripple epochs of all sites 200 times and calculating the mean number of co-occurrences for each proportion of co-rippling sites (i.e., the number of channels co-rippling divided by the total number of channels, assessed for the minimum value of 2 or more channels co-rippling).

Cortical ripple co-occurrence significance for each channel pair was computed by comparing the number of observed co-occurrences (25ms minimum overlap) for each channel pair with a null co-occurrence distribution derived from shuffling ripples and inter-ripple intervals 200 times in a moving non-overlapping 5min window and counting co-occurrences.

Ripple phase-locking and phase-lags

To evaluate the extent to which co-occurring ripples at different sites were synchronized at different times, we used the phase-locking value (PLV), an instantaneous measure of phase-locking[30]. PLV time courses were computed using the analytic angle of the Hilbert transformed 70-100Hz bandpassed (zero-phase shift) signals of each channel pair when there were at least 40 co-ripples with a minimum of 25ms overlap for each. PLVs were computed for all such co-ripples for each channel pair across a ±500ms window relative to the temporal centers of the co-ripples. A null distribution was generated by selecting 200 random times within -10 to -2 s relative to each co-ripple center. For plotting, PLV traces were smoothed with a 10ms Gaussian window. Pre-FDR p-values were determined by comparing the observed and null distributions in 5ms duration bins within ±50ms around the co-ripple centers. These p-values were then FDR corrected across bins and channel pairs. A channel pair was considered to have significant phase-locking if it had 2 consecutive bins with post-FDR $p<0.05$. Phase-locking modulation was computed for each channel pair as the difference from the average baseline PLV within -500 to -250ms to the max PLV within ±50ms around the co-ripple center. Phase-locking as a function of the proportion of additional sites co-rippling was computed by identifying co-ripples on the two cortical channels of interest, then sorting these events into groups based on what proportion of additional sites had a ripple that overlapped with the co-ripple by any amount of time, and computing the peak PLV around the co-ripple centers. Plots of the peak PLV for channel pairs as a function of the number of additional sites co-occurring (e.g., 3 on the x-axis means 2+3=5 total sites co-rippling) are for channel pairs with significant PLV modulations.

The phase-lag between co-occurring cortical ripples (25ms minimum overlap) was computed for channels with significant PLV modulations by finding the circular mean[80] of the angular difference between the two 70-100Hz bandpassed ripples during their overlapping period. The mean phase-lag for a given channel pair was computed by finding the circular mean of these circular means.

Statistical analyses

All statistical tests were evaluated with $\alpha=0.05$. All p-values involving multiple comparisons were FDR-corrected according to Benjamini and Hochberg (1995)[81]. FDR corrections across channel

pairs were done across all channels pairs from all patients included in the analysis. Box-and-whisker plots show median, mean, and interquartile range, with whiskers indicating 1.5 × interquartile range with outliers omitted. Significance of linear correlations were assessed using the significance of the correlation coefficient when there were at least 10 data points.

In temporal analyses (i.e., peri-ripple time histograms), p-values were corrected across bins and all channels. To compute p-values using randomization tests, the observed test statistic (e.g., events per bin) was compared to the null distribution of test statistics. Null distributions were randomly selected from the same epochs using 200 iterations. The p-value was computed as the proportion of null test statistics that were equal to or greater/less than the observed test statistic. Randomization tests were one-sided according to whether the observed test statistic was greater than or less than the mean of the null test statistics. Co-firing statistics were evaluated using a two-sided paired *t*-test to compare the observed to the mean of the null (either during 200 randomly selected non-ripple epochs matched in number and duration to the ripple epochs or during ripples with observed spike times shuffled 200 times) co-firing counts (between two different units; equal amount of time between observed and null) within 5ms across unit pairs. Order preferences (e.g., of ripples between channels) were assessed using a two-sided binomial test with an expected probability of 0.5. To determine if a circular distribution was non-uniform, the Hodges-Ajne test was used. To determine if two circular distributions had different circular means, a Watson-Williams multi-sample test was used. To test if co-rippling between two particular cortical sites made it more likely that additional cortical sites co-rippled, we computed a χ^2 test of proportions for all possible groups of three cortical channels under the null hypothesis that the co-occurrence of channel A and B has no relation to the co-occurrence of A and C. Each table was made from the number of ripples in A that co-occurred with a ripple in B only, or C only, or both, or neither, where A occurring with B or not B are the 2 rows, and A occurring with C or not C are the 2 columns. In the paired-associates memory analysis, chance ripple occurrences (or co-occurrences) were computed for each trial as the average of 200 random shuffles per channel (pair) within ±3s from recall onset. Only trials where there was a successful recall (of the same word pair) in both the immediate and ~60s delayed conditions were included. Linear mixed-effects models were performed with the patient as the random effect, as follows:

$$\textit{(co-)ripples} \sim \textit{condition} + (1 \mid \textit{patient}) \qquad (1)$$

Where *(co-)ripples* was the dependent variable computed as the average ripple rate (or co-ripple rate; minimum of 25ms overlap for each co-ripple) within 150-300ms following the stimulus cue preceding successful recall onset across trials, with the value for each trial as the average across channels, *condition* was 1) immediate recall or chance, 2) delayed recall or chance, 3) immediate recall or delayed recall (as a ratio of observed over chance), or 4) successful recall or unsuccessful recall (as a ratio of observed over chance).

Data availability

The de-identified raw data that support the findings of this study are available from the corresponding authors upon reasonable request provided that the data sharing agreement and patient consent permit that sharing.

Code availability

The code that support the findings of this study are available from the corresponding authors upon reasonable request.

References

1 Wilson, M. A. & McNaughton, B. L. Reactivation of hippocampal ensemble memories during sleep. *Science* **265**, 676-679 (1994).

2 Buzsaki, G. Hippocampal sharp wave-ripple: A cognitive biomarker for episodic memory and planning. *Hippocampus* **25**, 1073-1188, doi:doi:10.1002/hipo.22488 (2015).

3 Maingret, N., Girardeau, G., Todorova, R., Goutierre, M. & Zugaro, M. Hippocampo-cortical coupling mediates memory consolidation during sleep. *Nature Neuroscience* **19**, 959-964, doi:10.1038/nn.4304 (2016).

4 Ego-Stengel, V. & Wilson, M. A. Disruption of ripple-associated hippocampal activity during rest impairs spatial learning in the rat. *Hippocampus* **20**, 1-10, doi:10.1002/hipo.20707 (2009).

5 Ji, D. & Wilson, M. A. Coordinated memory replay in the visual cortex and hippocampus during sleep. *Nature Neuroscience* **10**, 100-107, doi:10.1038/nn1825 (2007).

6 Peyrache, A., Khamassi, M., Benchenane, K., Wiener, S. I. & Battaglia, F. P. Replay of rule-learning related neural patterns in the prefrontal cortex during sleep. *Nature Neuroscience* **12**, 919-926, doi:10.1038/nn.2337 (2009).

7 Johnson, L. A., Euston, D. R., Tatsuno, M. & McNaughton, B. L. Stored-trace reactivation in rat prefrontal cortex is correlated with down-to-up state fluctuation density. *J Neurosci* **30**, 2650-2661, doi:10.1523/JNEUROSCI.1617-09.2010 (2010).

8 Siapas, A. G. & Wilson, M. A. Coordinated interactions between hippocampal ripples and cortical spindles during slow-wave sleep. *Neuron* **21**, 1123-1128 (1998).

9 Latchoumane, C.-F. V., Ngo, H.-V. V., Born, J. & Shin, H.-S. Thalamic Spindles Promote Memory Formation during Sleep through Triple Phase-Locking of Cortical, Thalamic, and Hippocampal Rhythms. *Neuron* **95**, 424-435.e426, doi:10.1016/j.neuron.2017.06.025 (2017).

10 Staresina, B. P. *et al.* Hierarchical nesting of slow oscillations, spindles and ripples in the human hippocampus during sleep. *Nature Neuroscience* **18**, 1679-1686, doi:10.1038/nn.4119 (2015).

11 Jiang, X., Gonzalez-Martinez, J. & Halgren, E. Coordination of Human Hippocampal Sharpwave Ripples during NREM Sleep with Cortical Theta Bursts, Spindles, Downstates, and Upstates. *J Neurosci* **39**, 8744-8761, doi:10.1523/jneurosci.2857-18.2019 (2019).

12 Jiang, X., Gonzalez-Martinez, J. & Halgren, E. Posterior hippocampal spindle-ripples co-occur with neocortical theta-bursts and down-upstates, and phase-lock with parietal spindles during NREM sleep in humans. *J Neurosci*, 2858-2818, doi:10.1523/jneurosci.2858-18.2019 (2019).

13 Jiang, X. *et al.* Improved identification and differentiation from epileptiform activity of human hippocampal sharp wave ripples during NREM sleep. *Hippocampus* (2019).

14 Khodagholy, D., Gelinas, J. N. & Buzsáki, G. Learning-enhanced coupling between ripple oscillations in association cortices and hippocampus. *Science* **358**, 369-372, doi:10.1126/science.aan6203 (2017).

15 Grenier, F., Timofeev, I. & Steriade, M. Focal synchronization of ripples (80-200 Hz) in neocortex and their neuronal correlates. *J Neurophysiol* **86**, 1884-1898. (2001).

16 Vaz, A. P., Inati, S. K., Brunel, N. & Zaghloul, K. A. Coupled ripple oscillations between the medial temporal lobe and neocortex retrieve human memory. *Science* **363**, 975-978, doi:10.1126/science.aau8956 (2019).

17 Vaz, A. P., Wittig, J. H., Inati, S. K. & Zaghloul, K. A. Replay of cortical spiking sequences during human memory retrieval. *Science* **367**, 1131-1134 (2020).

18 Norman, Y. *et al.* Hippocampal sharp-wave ripples linked to visual episodic recollection in humans. *Science* **365**, eaax1030, doi:10.1126/science.aax1030 (2019).

19 Mukamel, R. *et al.* Coupling between neuronal firing, field potentials, and FMRI in human auditory cortex. *Science* **309**, 951-954, doi:10.1126/science.1110913 (2005).
20 Rosen, B. Q. & Halgren, E. A whole-cortex probabilistic diffusion tractography connectome. *eNeuro*, ENEURO.0416-0420.2020, doi:10.1523/eneuro.0416-20.2020 (2021).
21 Gonzalez, C. E. *et al.* Theta bursts precede, and spindles follow, cortical and thalamic downstates in human NREM sleep. *J Neurosci* **38**, 9989-10001 (2018).
22 Mak-McCully, R. A. *et al.* Coordination of cortical and thalamic activity during non-REM human sleep. *Nature Communications* (2017).
23 Csercsa, R. *et al.* Laminar analysis of slow wave activity in humans. *Brain* **133**, 2814-2829, doi:10.1093/brain/awq169 (2010).
24 Dickey, C. W. *et al.* Travelling spindles create necessary conditions for spike-timing-dependent plasticity in humans. *Nature Communications* **12**, 1027, doi:10.1038/s41467-021-21298-x (2021).
25 Bazhenov, M., Rulkov, N. F. & Timofeev, I. Effect of synaptic connectivity on long-range synchronization of fast cortical oscillations. *J Neurophysiol* (2008).
26 Rasch, B. & Born, J. About sleep's role in memory. *Physiol Rev* **93**, 681-766, doi:10.1152/physrev.00032.2012 (2013).
27 Jiang, X. *et al.* Replay of large-scale spatio-temporal patterns from waking during subsequent NREM sleep in human cortex. *Scientific Reports* **7**, 17380, doi:10.1038/s41598-017-17469-w (2017).
28 Felleman, D. J. & VanEssen, D. C. Distributed hierarchical processing in the primate cerebral cortex. *Cerebral Cortex* **1**, 1-47 (1991).
29 Fries, P. Neuronal Gamma-Band Synchronization as a Fundamental Process in Cortical Computation. *Annual Review of Neuroscience* **32**, 209-224, doi:10.1146/annurev.neuro.051508.135603 (2009).
30 Lachaux, J. P., Rodriguez, E., Martinerie, J. & Varela, F. J. Measuring phase synchrony in brain signals. *Hum Brain Mapp* **8**, 194-208, doi:10.1002/(sici)1097-0193(1999)8:4<194::aid-hbm4>3.0.co;2-c (1999).
31 Stark, E. *et al.* Pyramidal cell-interneuron interactions underlie hippocampal ripple oscillations. *Neuron* **83**, 467-480, doi:10.1016/j.neuron.2014.06.023 (2014).
32 Buzsáki, G. & Wang, X. J. Mechanisms of gamma oscillations. *Annu Rev Neurosci* **35**, 203-225, doi:10.1146/annurev-neuro-062111-150444 (2012).
33 Bartos, M. *et al.* Fast synaptic inhibition promotes synchronized gamma oscillations in hippocampal interneuron networks. *Proceedings of the National Academy of Science* **99**, 13222-13227. (2002).
34 Feldman, D. E. The spike-timing dependence of plasticity. *Neuron* **75**, 556-571 (2012).
35 Halgren, E. in *Neurobiology of Cognition* (eds A. Scheibel & A. Weschsler) 103-150 (Guilford, 1990).
36 Simić, G., Kostović, I., Winblad, B. & Bogdanović, N. Volume and number of neurons of the human hippocampal formation in normal aging and Alzheimer's disease. *J Comp Neurol* **379**, 482-494, doi:10.1002/(sici)1096-9861(19970324)379:4<482::aid-cne2>3.0.co;2-z (1997).
37 Azevedo, F. A. *et al.* Equal numbers of neuronal and nonneuronal cells make the human brain an isometrically scaled-up primate brain. *Journal of Comparative Neurology* **513**, 532-541 (2009).
38 Vicente, R., Gollo, L. L., Mirasso, C. R., Fischer, I. & Pipa, G. Dynamical relaying can yield zero time lag neuronal synchrony despite long conduction delays. *Proceedings of the National Academy of Sciences* **105**, 17157-17162 (2008).
39 Salinas, E. & Sejnowski, T. J. Correlated neuronal activity and the flow of neural information. *Nat Rev Neurosci* **2**, 539-550 (2001).

40 Treisman, A. Solutions to the binding problem: progress through controversy and convergence. *Neuron* **24**, 105-110, 111-125 (1999).
41 Singer, W. Neuronal synchrony: a versatile code for the definition of relations? *Neuron* **24**, 49-65, 111-125 (1999).
42 Merker, B. Cortical gamma oscillations: the functional key is activation, not cognition. *Neuroscience & Biobehavioral Reviews* **37**, 401-417 (2013).
43 Shadlen, M. N. & Movshon, J. A. Synchrony unbound: a critical evaluation of the temporal binding hypothesis. *Neuron* **24**, 67-77, 111-125 (1999).
44 Eichenbaum, H. & Cohen, N. J. Can we reconcile the declarative memory and spatial navigation views on hippocampal function? *Neuron* **83**, 764-770 (2014).
45 Patel, J., Schomburg, E. W., Berényi, A., Fujisawa, S. & Buzsáki, G. Local Generation and Propagation of Ripples along the Septotemporal Axis of the Hippocampus. *J Neurosci* **33**, 17029-17041, doi:10.1523/jneurosci.2036-13.2013 (2013).
46 Fernández, E. *et al.* Acute human brain responses to intracortical microelectrode arrays: challenges and future prospects. *Frontiers in Neuroengineering* **7**, doi:10.3389/fneng.2014.00024 (2014).
47 Keller, C. J. *et al.* Heterogeneous neuronal firing patterns during interictal epileptiform discharges in the human cortex. *Brain* **133**, 1668-1681, doi:10.1093/brain/awq112 (2010).
48 Waziri, A. *et al.* Initial surgical experience with a dense cortical microarray in epileptic patients undergoing craniotomy for subdural electrode implantation. *Neurosurgery* **64**, 540-545; discussion 545, doi:10.1227/01.NEU.0000337575.63861.10 (2009).
49 Oostenveld, R., Fries, P., Maris, E. & Schoffelen, J. M. FieldTrip: Open source software for advanced analysis of MEG, EEG, and invasive electrophysiological data. *Comput Intell Neurosci* **2011**, 156869, doi:10.1155/2011/156869 (2011).
50 Mak-McCully, R. A. *et al.* Distribution, Amplitude, Incidence, Co-Occurrence, and Propagation of Human K-Complexes in Focal Transcortical Recordings. *eNeuro* **2**, doi:10.1523/eneuro.0028-15.2015 (2015).
51 Fischl, B. FreeSurfer. *Neuroimage* **62**, 774-781, doi:10.1016/j.neuroimage.2012.01.021 (2012).
52 Fischl, B. *et al.* Automatically parcellating the human cerebral cortex. *Cereb Cortex* **14**, 11-22, doi:10.1093/cercor/bhg087 (2004).
53 Destrieux, C., Fischl, B., Dale, A. & Halgren, E. Automatic parcellation of human cortical gyri and sulci using standard anatomical nomenclature. *Neuroimage* **53**, 1-15, doi:10.1016/j.neuroimage.2010.06.010 (2010).
54 Iglesias, J. E. *et al.* A computational atlas of the hippocampal formation using ex vivo, ultra-high resolution MRI: Application to adaptive segmentation of in vivo MRI. *Neuroimage* **115**, 117-137, doi:10.1016/j.neuroimage.2015.04.042 (2015).
55 Johnson, H., Harris, G. & Williams, K. BRAINSFIT: Mutual information registrations of whole-brain 3D Images, using the insight toolkit. (2007).
56 Fedorov, A. *et al.* 3D Slicer as an image computing platform for the Quantitative Imaging Network. *Magn Reson Imaging* **30**, 1323-1341, doi:10.1016/j.mri.2012.05.001 (2012).
57 Fischl, B., Sereno, M. I., Tootell, R. B. & Dale, A. M. High-resolution intersubject averaging and a coordinate system for the cortical surface. *Hum Brain Mapp* **8**, 272-284, doi:10.1002/(sici)1097-0193(1999)8:4<272::aid-hbm10>3.0.co;2-4 (1999).
58 Glasser, M. F. *et al.* A multi-modal parcellation of human cerebral cortex. *Nature* **536**, 171-178, doi:10.1038/nature18933 (2016).
59 Behrens, T. E. J., Berg, H. J., Jbabdi, S., Rushworth, M. F. S. & Woolrich, M. W. Probabilistic diffusion tractography with multiple fibre orientations: What can we gain? *NeuroImage* **34**, 144-155, doi:10.1016/j.neuroimage.2006.09.018 (2007).

60 Desikan, R. S. *et al.* An automated labeling system for subdividing the human cerebral cortex on MRI scans into gyral based regions of interest. *NeuroImage* **31**, 968-980 (2006).
61 Delorme, A. & Makeig, S. EEGLAB: an open source toolbox for analysis of single-trial EEG dynamics including independent component analysis. *J Neurosci Methods* **134**, 9-21, doi:10.1016/j.jneumeth.2003.10.009 (2004).
62 Axmacher, N., Elger, C. E. & Fell, J. Ripples in the medial temporal lobe are relevant for human memory consolidation. *Brain* **131**, 1806-1817 (2008).
63 Le Van Quyen, M. *et al.* Cell Type-Specific Firing during Ripple Oscillations in the Hippocampal Formation of Humans. *J Neurosci* **28**, 6104-6110, doi:10.1523/jneurosci.0437-08.2008 (2008).
64 Clemens, Z. *et al.* Temporal coupling of parahippocampal ripples, sleep spindles and slow oscillations in humans. *Brain* **130**, 2868-2878, doi:10.1093/brain/awm146 (2007).
65 Staba, R. J. *et al.* High-frequency oscillations recorded in human medial temporal lobe during sleep. *Annals of Neurology* **56**, 108-115, doi:doi:10.1002/ana.20164 (2004).
66 Bragin, A., Engel, J., Jr., Wilson, C. L., Fried, I. & Buzsaki, G. High-frequency oscillations in human brain. *Hippocampus* **9**, 137-142 (1999).
67 Eichenlaub, J.-B. *et al.* Replay of Learned Neural Firing Sequences during Rest in Human Motor Cortex. *Cell Reports* **31**, 107581 (2020).
68 Teleńczuk, B. *et al.* Local field potentials primarily reflect inhibitory neuron activity in human and monkey cortex. *Scientific reports* **7**, 40211 (2017).
69 Le Van Quyen, M. *et al.* High-frequency oscillations in human and monkey neocortex during the wake–sleep cycle. *Proceedings of the National Academy of Sciences* **113**, 9363-9368 (2016).
70 Dehghani, N. *et al.* Dynamic balance of excitation and inhibition in human and monkey neocortex. *Scientific Reports* **6** (2016).
71 Chan, A. M. *et al.* Speech-specific tuning of neurons in human superior temporal gyrus. *Cereb Cortex* **24**, 2679-2693, doi:10.1093/cercor/bht127 (2014).
72 Peyrache, A. *et al.* Spatiotemporal dynamics of neocortical excitation and inhibition during human sleep. *Proceedings of the National Academy of Science* **109**, 1731-1736, doi:10.1073/pnas.1109895109 (2012).
73 Kamiński, J., Brzezicka, A., Mamelak, A. N. & Rutishauser, U. Combined Phase-Rate Coding by Persistently Active Neurons as a Mechanism for Maintaining Multiple Items in Working Memory in Humans. *Neuron* **106**, 256-264.e253, doi:10.1016/j.neuron.2020.01.032 (2020).
74 Pouzat, C., Mazor, O. & Laurent, G. Using noise signature to optimize spike-sorting and to assess neuronal classification quality. *Journal of Neuroscience Methods* **122**, 43-57, doi:10.1016/S0165-0270(02)00276-5 (2002).
75 Hagler, D. J., Jr. *et al.* Heterogeneous Origins of Human Sleep Spindles in Different Cortical Layers. *J Neurosci* **38**, 3013-3025, doi:10.1523/jneurosci.2241-17.2018 (2018).
76 Müllner, D. fastcluster: Fast hierarchical, agglomerative clustering routines for R and Python. *Journal of Statistical Software* **53**, 1-18 (2013).
77 Langfelder, P., Zhang, B. & Horvath, S. Defining clusters from a hierarchical cluster tree: the Dynamic Tree Cut package for R. *Bioinformatics* **24**, 719-720, doi:10.1093/bioinformatics/btm563 (2008).
78 Miller, J.-e. K., Ayzenshtat, I., Carrillo-Reid, L. & Yuste, R. Visual stimuli recruit intrinsically generated cortical ensembles. *Proceedings of the National Academy of Sciences* **111**, E4053-E4061 (2014).
79 Gabadinho, A., Ritschard, G., Mueller, N. S. & Studer, M. Analyzing and visualizing state sequences in R with TraMineR. *Journal of Statistical Software* **40**, 1-37 (2011).

80 Berens, P. CircStat: A MATLAB Toolbox for Circular Statistics. *Journal of Statistical Software* **31**, 1-21, doi:10.18637/jss.v031.i10 (2009).

81 Benjamini, Y. & Hochberg, Y. Controlling the false discovery rate: a practical and powerful approach to multiple testing. *Journal of the Royal statistical society: series B (Methodological)* **57**, 289-300 (1995).